Identification of an antiretroviral small molecule that appears to be a host-targeting inhibitor of HIV-1 assembly

Jonathan C. Reed[a], Dennis Solas[b], Anatoliy Kitaygorodskyy[b], Beverly Freeman[b], Dylan T. B. Ressler[a], Daryl J. Phuong[a], J. Victor Swain[a], Kent Matlack, Clarence R. Hurt, Vishwanath R. Lingappa[b], and Jaisri R. Lingappa[a]#

[a]Dept. of Global Health, University of Washington, Seattle, WA. 98109

[b]Prosetta Biosciences, San Francisco, CA 94107

Running Head: Host-targeting inhibitor of HIV-1 assembly

#Address correspondence to Jaisri R. Lingappa, jais@uw.edu.

Word count in abstract: 249

Word count in text: 6079

ABSTRACT

Given the projected increase in multidrug resistant HIV-1, there is an urgent need for development of antiretrovirals that act on virus life-cycle stages that are not targeted by antiretrovirals currently in use. Host-targeting drugs are of particular interest because they can offer a high barrier to resistance. Here we report identification of two related small molecules that inhibit HIV-1 late events, a stage of the HIV-1 life cycle for which potent and specific inhibitors are lacking. This chemotype was discovered using cell-free protein synthesis and assembly systems that recapitulate intracellular host-catalyzed viral capsid assembly pathways. These compounds inhibit replication of HIV-1 in human T cell lines and PBMCs and are effective against a primary isolate. They reduce virus production, likely by inhibiting a post-translational step in HIV-1 Gag assembly. Notably, the compound colocalizes with HIV-1 Gag *in situ*; however, unexpectedly, selection experiments failed to identify compound-specific resistance mutations in *gag* or *pol*, even though known resistance mutations developed in a parallel nelfinavir selection. Thus, we hypothesized that instead of binding to Gag directly, these compounds might localize to assembly intermediates, the intracellular multiprotein complexes containing Gag and host factors that are formed during immature HIV-1 capsid assembly. Indeed, imaging of infected cells showed colocalization of the compound with two host enzymes found in assembly intermediates, ABCE1 and DDX6. While the exact target and mechanism of action of this chemotype remain to be determined, these findings suggest that these compounds represent first-in-class, host-targeting inhibitors of intracellular events in HIV-1 assembly.

51 **IMPORTANCE**

52 The success of antiretroviral treatment for HIV-1 is at risk of being undermined by the growing problem
53 of drug resistance. Thus, there is a need to identify antiretrovirals that act on viral life cycle stages not
54 targeted by drugs in use, such as the events of HIV-1 Gag assembly. To address this gap, we developed
55 a compound screen that recapitulates the intracellular events of HIV-1 assembly, including viral-host
56 interactions that promote assembly. This effort led to identification of a new chemotype that inhibits
57 HIV-1 replication at nanomolar concentrations by inhibiting virus production. This compound
58 colocalized with Gag and two host enzymes that facilitate capsid assembly but resistance selection did
59 not result in compound-specific mutations in *gag,* suggesting that the chemotype does not directly target
60 Gag. We hypothesize that this chemotype may represent a first-in-class inhibitor of virus production
61 that acts by targeting a viral-host complex important for HIV-1 Gag assembly.
62
63
64
65
66
67
68
69
70
71
72
73
74
75

76 **INTRODUCTION**

77 In an era in which HIV-1 vaccine trial results have been disappointing, antiretroviral (ARV) drugs
78 stand out as a stunning success story. Treatment with combined antiretroviral therapy (ART) over the
79 past three decades has resulted in enormous reductions in morbidity and mortality from HIV-1 infection,
80 with 62% of the 38 million people living with HIV receiving antiretroviral drugs in 2018 (1). ART is
81 also the mainstay of PREP, a remarkably successful approach to preventing HIV-1 infection (1, 2).
82 Additionally, ART will be important for future HIV cure strategies. Unfortunately, the success of HIV
83 ART is at risk of being undermined by the increasingly serious problem of HIV-1 drug resistance (3).
84 Virologic failure is seen in up to 20% of individuals receiving first-line ART in low and middle-income
85 countries (4), with up to half of first-line ART failures in sub-Saharan Africa involving resistance to all
86 three drugs in tenofovir-containing regimens (5). Moreover, the prevalence of drug-resistant HIV-1 is
87 predicted to increase substantially over time as more people receive treatment (6). Indeed, experts have
88 drawn analogies between the future of ART and the current crisis of multidrug resistant tuberculosis (7).
89 For this reason, identifying novel targets in the HIV-1 life cycle and candidate small molecules that
90 inhibit these targets is a high priority, with the goal of driving development of new ARV drugs.

91 Identification of new druggable targets in the poorly understood stages of the viral life cycle will be
92 particularly important for development of drugs aimed at HIV-1 strains resistant to currently available
93 drugs. Mapping the targets of drugs currently in use onto the HIV-1 life cycle reveals a striking lack of
94 drugs that target intracellular events of assembly (8). Currently available ARV drugs target the
95 maturation, entry, and post-entry stages of the viral life cycle. In contrast, no approved ARV drugs
96 target intracellular viral late events (purple bar in Fig. 1A), which include post-translational events of
97 immature capsid assembly. Formation of a single infectious virus requires assembly of ~3000 copies of
98 the HIV-1 Gag protein, which are synthesized and oligomerize in the cytoplasm and subsequently target
99 to the plasma membrane, where they encapsidate the HIV-1 genome while multimerizing to form the
100 immature capsid. The immature capsid then undergoes budding, release, and maturation (Fig. 1A).

101 Interest in targeting HIV-1 assembly has been high, leading to numerous drug screens in recent years (9,
102 10). Of the compounds identified in these screens, the most successful have been those that bind to the
103 capsid protein (CA). CA is critical at multiple stages of the viral life cycle including immature capsid
104 assembly, maturation, infectivity, and post-entry events. Interestingly, potent small molecules that
105 target CA do not selectively inhibit immature capsid assembly (reviewed in (9)) – instead they either act
106 preferentially on the mature capsid, targeting virion infectivity and post-entry events (e.g. PF74 (11-
107 16)), or act broadly on Gag synthesis, assembly, and post-entry events (e.g. GS-CA1 (17)) (Fig. 1A).
108 Indeed, to our knowledge, there are no reports of a potent small molecule identified in any screen that
109 selectively inhibits intracellular HIV-1 late events.

110 We hypothesized that one reason for the failure to identify potent and selective inhibitors of HIV-1
111 assembly might be that previous screens were either very broad or very narrow – i.e. they encompassed
112 the entire viral life cycle (e.g.(12, 18)) or they were based solely on multimerization of recombinant CA-
113 derived peptides *in vitro* (e.g.(19-22)). We further hypothesized that a screen that focuses only on
114 events of Gag assembly but includes known cellular facilitators of immature HIV-1 capsid assembly
115 could be more successful than other screens in identifying a potent and selective inhibitor of intracellular
116 events in HIV-1 assembly. Specifically, while recombinant Gag is able to assemble into immature
117 capsid-like particles in the absence of host proteins (reviewed in (23)), two decades of studies support a
118 different model for HIV-1 assembly in cells – one in which Gag assembles into immature capsids via a
119 pathway of assembly intermediates containing viral proteins as well as host proteins that act catalytically
120 to promote HIV-1 capsid assembly (e.g. (24-34); Fig. 1B). This model suggests that to succeed in the
121 hostile environment of the cytoplasm, Gag may have evolved to utilize host proteins to catalyze Gag
122 multimerization, promote RNA packaging, and sequester assembly within host complexes where
123 nascent virions would be less vulnerable to host defenses. If this host-catalyzed model of capsid
124 assembly in the cytoplasm is valid, then a screen that recapitulates this pathway might succeed in
125 identifying new druggable targets.

126 Indeed, a precedent exists for a screen that recapitulates a host-catalyzed assembly pathway enabling
127 identification of a novel antiviral compound and target. Previously our group, in collaboration with
128 investigators at the Centers for Disease Control and Prevention, used a cell-extract-based screen that
129 recapitulated an intracellular assembly pathway for rabies virus (RABV) to identify the first reported
130 small molecule inhibitor of RABV replication in cell culture (35). Notably, this small molecule binds to
131 a multiprotein complex that contains ATP-binding cassette protein E1 (ABCE1), a host enzyme
132 identified in HIV-1 assembly intermediates, suggesting that similar host complexes may be involved in
133 the assembly of diverse viruses.
134 Motivated by the RABV precedent, we developed cell-extract-based assembly pathway screens for
135 other viruses and used them to identify a novel and potent antiretroviral chemotype that inhibits HIV-1
136 replication, represented by the small molecule PAV-117 and its more potent analog PAV-206. Here we
137 present evidence suggesting that this chemotype inhibits HIV-1 replication by interfering with HIV-1
138 assembly. We found that a tagged analog of these compounds colocalizes with Gag *in situ*, suggesting
139 that they may target HIV-1 Gag. However, surprisingly, compound-specific mutations did not arise in
140 *gag* or *pol* after 37 weeks of PAV-206 selection in HIV-1-infected human cells, in stark contrast to
141 nelfinavir selection examined in parallel, arguing against Gag being the direct target of PAV-206.
142 Additional imaging studies shed more light on our failure to identify viral resistance mutations by
143 demonstrating that the tagged PAV-206 analog also colocalizes with two host proteins associated with
144 Gag in intracellular HIV-1 capsid assembly intermediates, the enzymes ABCE1 and DEAD-box helicase
145 6 (DDX6). While the exact target and mechanism of action of PAV-117/PAV-206 remain unclear, these
146 studies raise the possibility that they represent a class of novel host-targeting ARV small molecules that
147 inhibits HIV-1 virus production by acting on host-protein-containing capsid assembly intermediates.
148
149
150

151 **RESULTS**

152 **Development of a novel screen for HIV-1 assembly inhibitors based on previous studies of the**
153 **intracellular HIV-1 capsid assembly pathway**

154 Our interest in using the cell-free assembly system as a drug screen stems from an early study that
155 utilized this system to generate the first evidence that immature HIV-1 capsids assemble via a host-
156 catalyzed pathway of intermediates (28). Adapted from the *in vitro* protein synthesis systems that were
157 used to identify signal sequences (36), the cell-free HIV-1 assembly system supports *de novo* synthesis
158 of HIV-1 Gag polypeptides from a Gag mRNA using energy substrates, amino acids, and a cellular
159 extract that provides host factors required for Gag translation as well as post-translational events of Gag
160 assembly. When programmed with wild-type Gag mRNA, this system produces particles that closely
161 resemble completed immature HIV-1 capsids produced by provirus-expressing cells, judging by their
162 ultrastructural appearance as well as in their size and shape (as defined by a sedimentation value of
163 ~750S; (28)). Pulse-chase studies in cell-free assembly reactions revealed sequential progression of Gag
164 through complexes of increasing size (~10S to ~80S/150S to ~500S to ~750S), consistent with these
165 smaller complexes being intermediates in the formation of the ~750S completely assembled immature
166 capsid. Moreover, Gag mutants that had been defined by others to be assembly-defective in cells are
167 arrested at specific steps of the cell-free assembly pathway, with assembly-competent Gag mutants
168 progressing through the entire pathway (28, 37). Notably, biochemical analysis demonstrated that post-
169 translational events in this assembly pathway required ATP, indicating that HIV-1 immature capsid
170 assembly in cells is energy-dependent (28).

171 While initially identified in a cell-free system, the HIV-1 capsid assembly pathway has been largely
172 studied in cellular systems in the last two decades. Key features of the assembly pathway were validated
173 in cells expressing the HIV-1 provirus (reviewed in (32)), including the sequential progression of Gag
174 through the pathway of assembly intermediates (26, 32), the energy dependence of the pathway (25),
175 and the arrest of known assembly-defective Gag mutants at specific steps in the pathway (25-28, 32, 33,

176 38). The energy dependence of immature capsid assembly, which has been confirmed by other groups
177 (39), was subsequently explained by the finding that the assembly intermediates contain at least two host
178 enzymes that facilitate assembly - the ATPase ABCE1 and the RNA helicase DDX6 (30, 34). Other
179 studies suggest that packaging of the HIV-1 genome appears to occur in the assembly intermediates (24,
180 32), and that other lentiviruses utilize analogous assembly pathways (25, 31). Immunoprecipitation and
181 imaging studies confirmed the association of ABCE1 and DDX6 with assembling Gag and identified
182 two other enzymes in assembly intermediates, AGO2 and DCP2 (24, 26, 27, 30-33). The finding that
183 assembly intermediates contain proteins typically found in host RNA granules, e.g. DDX6, AGO2, and
184 DCP2, supports a model in which assembling Gag co-opts a unique subclass of host ribonucleoprotein
185 (RNP) complexes that are related to RNA granules but differ from well-studied RNA granules such as P
186 bodies and stress granules. RNA granules are a diverse group of ribonucleoprotein complexes involved
187 in all aspects of host RNA metabolism except protein synthesis. Sequestration of immature HIV-1
188 capsid assembly events in such host RNP complexes could allow HIV-1 assembly to be protected from
189 the innate immune system while at the same time allowing assembling Gag access to the viral genome,
190 which is found in these complexes (24, 32), and to utilize enzymes that could facilitate packaging and
191 assembly (Fig. 1B).
192 While the cellular studies described above demonstrated the physiological relevance of the HIV-1
193 assembly pathway, we reasoned that the cell-free system in which it was identified could hold promise
194 as a drug screen. A cell-free assembly drug screen would have the advantage of recapitulating
195 evolutionarily conserved viral-host interactions critical for assembly while being much less expensive
196 than drug screens that utilize infected cell lines in culture. Additionally, the cell-free system can be
197 adapted for a moderately high-throughput format. Together, these features of a cell-free assembly
198 pathway drug screen allow a large number of compounds to be screened in a cost-effective manner.
199 For these reasons, we adapted the HIV-1 cell-free assembly reaction to generate a drug screen (Fig.
200 1C) similar to the RABV drug screen (35). Cell free reactions, upon completion, contain assembly

201 intermediates and fully assembled immature capsid-like particles, unless performed in the presence of an
202 inhibitor of assembly, in which case Gag will be largely unassembled (i.e. monomers and dimers).
203 Plate-bound anti-Gag antibodies capture monomeric, dimeric, and multimerized Gag from the reaction.
204 To determine how much Gag multimerization occurred during the reaction, a soluble anti-Gag detection
205 antibody is added. The detection antibody does not bind Gag monomers (since the monomer antigenic
206 site is already bound by capture antibody) but would be expected to bind to unoccupied Gag proteins in
207 multimers. Signal from bound detection antibody is quantified using a fluorescent detection system,
208 with more signal being generated by Gag multimers. Thus, an effective inhibitor of Gag
209 multimerization will be recognized by a reduction in detection antibody signal (Fig. 1C). Because we
210 are interested in inhibitors of assembly rather than protein synthesis, we utilized a counter screen to
211 eliminate from further consideration all small molecules that inhibit translation of GFP in cell-free
212 reactions.
213
214 **Identification of a potent inhibitor of HIV-1 replication**
215 Once this cell-free HIV-1 assembly screen and counter screen were successfully established and
216 validated, similar cell-free screens were established for quantifying assembly of the capsids of seven
217 other viruses (Fig. 2A). A compound library of ~150,000 small molecules with drug-like characteristics
218 was screened against these eight cell-free assembly assays, resulting in a master hit collection of 249
219 small molecules that inhibited assembly in one or more virus assembly screen(s), but did not
220 significantly inhibit GFP translation.
221 Compounds in the master hit collection were further screened for their ability to inhibit replication of
222 HIV-1 in the MT-2 human T cell line. The compound with the most favorable characteristics in this
223 assay was PAV-117, a tetrahydroisoquinolone derivative with excellent drug-like properties (Fig. 2B).
224 PAV-117 inhibits replication of HIV-1 NL4-3 in MT-2 cells with a 50% reduction in virus replication
225 (EC50) of 48 nM and a 50% reduction in cell viability (CC50) of 1.0 μM (Fig. 2C). The nanomolar

226 EC50 and a selectivity index (CC50/EC50) of 21 make PAV-117 an excellent compound for further
227 optimization. Notably, PAV-117 was not active against influenza A virus WSN/33 [H1N1] (FLUV)
228 suggesting that it is not an antiviral that acts broadly on all enveloped viruses (Fig. 2D). Moreover,
229 PAV-117 was also relatively inactive against feline immunodeficiency virus (FIV), a non-primate
230 lentivirus that is related to HIV-1, indicating specificity even among lentiviruses (Fig. 2E). PAV-117
231 was active against a primary isolate of HIV-1 (Fig. 2F), indicating that its antiretroviral activity is not
232 restricted to laboratory isolates of HIV-1.
233
234 **Defining the step in the viral life cycle at which the novel small molecule acts**
235 Since other types of assembly inhibitor screens had identified compounds that act on viral early
236 events as described above, we next asked whether PAV-117 inhibits HIV-1 replication by acting on
237 entry or post-entry events in the HIV-1 life cycle. For this assay, we infected MT-2 cells, in the
238 presence of PAV-117 or DMSO, with a luciferase-encoding HIV-1 reporter virus (HIV-1 pNL4-3 RLuc
239 Δ*env*) that is pseudotyped with HIV-1 Env and undergoes only one round of replication (Fig. 3A,
240 diagram). At non-toxic concentrations, PAV-117 did not reduce luciferase activity in this assay (Fig.
241 3A, graph; EC50 of 930 nM; CC50 of 1.1 μM), indicating that it does not act on early events in the
242 HIV-1 life cycle. The effect of PAV-117 on viral late events (events that occur after integration) was
243 assayed using chronically infected H9 T cells, which produce infectious virus from integrated HIV-1
244 provirus (Fig. 3B, diagram). In this assay, PAV-117 inhibited production of infectious virus in the
245 culture supernatant, with an EC50 of 104 nM (Fig. 3B, black dose-response curve in graph). Thus,
246 PAV-117 activity can be entirely attributed to inhibition of viral late events. To determine whether
247 PAV-117 results in production of virus-like particles (VLP) that were non-infectious, we quantified
248 production of p24 Gag in VLP pelleted from cell culture supernatants of chronically infected H9 cells
249 treated with PAV-117 or DMSO. Finding that PAV-117 reduces virus infectivity without altering the
250 amount of p24 Gag in virus pellets would indicate that PAV-117 results in production of non-infectious

251 VLP. However, what we actually observed was the opposite - that inhibition of p24 production was
252 similar to inhibition of supernatant infectivity (EC50 of 113 nM vs. 104 nM, respectively; compare blue
253 vs. black curve in Fig. 3B graph), indicating that the compound blocks virus production. Western blots
254 of VLP in supernatants also showed no obvious change in the ratio of p55 to p24 with increasing PAV-
255 117 concentration relative to DMSO treatment (Fig. 3B, blot), arguing that it does not act on Gag
256 cleavage required for virus maturation.

257 The finding that the entire effect of PAV-117 is due to inhibition of virus production (Fig. 3)
258 indicated that PAV-117 likely acts on an intracellular viral late event. Such events include transcription
259 of the full-length HIV-1 mRNA, translation of this mRNA to produce Gag and GagPol, assembly of Gag
260 to produce immature capsids, and budding at the plasma membrane to release immature virus. We
261 hypothesized that PAV-117 likely acts on post-translational events in assembly of immature HIV-1
262 capsids for two reasons: first, because a counter screen had been utilized to eliminate inhibitors of
263 translation; and second, because the cell-free screens that identified PAV-117 recapitulate capsid protein
264 assembly but not virus budding and release. To test this hypothesis, we analyzed acutely infected MT-2
265 cells that had been treated for 48 h with DMSO or PAV-117 at 0.25 nM vs. 0.75 nM (~EC70 and
266 ~EC90). As expected, we observed a dose-dependent reduction in p24 release into the supernatant (Fig.
267 4A). Consistent with PAV-117 not being an inhibitor of translation, steady-state levels of actin and
268 GAPDH were minimally affected (Fig. 4B). At the highest PAV-117 concentration tested, some
269 reduction in steady-state Gag levels was observed (Fig. 4A), but it was much less than the reduction in
270 VLP production. To further define where PAV-117 acts, we also examined steady-state levels of HIV-1
271 capsid assembly intermediates, whose distinct S values allow them to be separated by velocity
272 sedimentation. PAV-117 had little to no effect on steady-state levels, as % of total Gag, of the ~10S and
273 ~80S/150S intermediates but resulted in a dose-dependent decrease in the steady-state level of the
274 ~500S intermediate (Fig. 4C). While the steady-state data in Fig. 4 provide a snapshot of intracellular
275 Gag levels at only one point in time, taken together with the dramatic reduction in cumulative VLP

276 production (across 48 h) in Fig. 3B, these data suggest that PAV-117 acts during virus assembly, most
277 likely by inhibiting formation of the ~500S assembly intermediate.
278
279 **Generation of analogs of the novel small molecule inhibitor that are more potent or contain a tag**
280 If PAV-117 acts during assembly, one might expect it to be associated with assembling HIV-1 Gag.
281 To test if this is the case, we needed an analog of PAV-117 that contains a tag, such as biotin, to allow
282 detection while retaining antiviral activity. To identify positions that could be used for a biotin tag,
283 structure-activity relationships were analyzed with combinations of methyl, methoxy, or benzoyloxy
284 substitutions in the R1, R2, and R3 positions of the pendant benzene ring (Fig. 5A). Interestingly, we
285 observed that the presence of a methyl in the R1 position and a methoxy in the R2 position (PAV218
286 and PAV-206) resulted in reduced toxicity (higher CC50) and a higher selectivity index when analyzed
287 in HIV-1 infected MT-2 T cells (Fig. 5A). PAV-206, which differs from PAV-117 only because it
288 contains a methoxy rather than a benzoyloxy group in the R3 position, was particularly notable since it
289 had a lower EC50 and higher CC50 than PAV-117, resulting in an excellent average SI of 61 in MT-2
290 cells (Fig. 5A, B) and 48 in HIV-1 infected PBMCs (Fig. 5B).
291 In addition to identifying PAV-206, a more potent analog of PAV-117, the structure-activity
292 relationship analysis led to a strategy for introducing a tag into PAV-117 (or PAV-206) by revealing that
293 the R3 position can tolerate either a bulky group (as in PAV-117) or a hydrogen (as in PAV218) without
294 significant loss of activity (Fig. 5A). For this reason, we introduced a biotin at this position, generating
295 the PAV-818 analog (Fig. 5C), which is identical to PAV-117 and PAV-206 except at the R3 position.
296 PAV-818 has a higher EC50 (951 nM) than the PAV-117 or PAV-206 analogs, but also has a higher
297 CC50 (~30 μM), generating an SI of ~32 (Fig. 5C), which is slightly better than the SI of PAV-117.
298 Thus, PAV-818 represents a biotinylated analog of PAV-206 and PAV-117 that can be utilized to
299 visualize where these compounds localize within infected cells.
300

301 **A tagged analog of PAV-206 colocalizes with HIV-1 Gag *in situ* in infected cells**

302 Next we utilized the biotinylated antiviral analog PAV-818 to ask if this family of compounds
303 colocalizes with HIV-1 Gag as one would expect if they inhibit assembly, as suggested by data in Figs. 3
304 and 4. For this purpose, we used the proximity ligation assay (PLA), a technique which marks two
305 antigens that are in close proximity with fluorescent spots. Briefly, in PLA, primary antibodies from
306 two species are detected by species-specific secondary antibodies that are tagged with oligonucleotides.
307 These oligonucleotides hybridize to connector oligonucleotides only if the antigens detected by the
308 primary antibodies are within ~40 nm of each other. Ligation of connector oligonucleotides and
309 addition of a polymerase results in rolling circle amplification to generate a sequence that can be
310 detected by a complementary oligonucleotide conjugated to a fluorescent probe (40). Thus, the
311 fluorescent spots (in this case, red spots) represent sites where two antigens are colocalized. To
312 determine whether PAV-818 colocalizes with HIV-1 Gag, we performed biotin-Gag PLA on 293T cells
313 that were chronically infected with HIV-1 and treated with either the biotinylated antiretroviral PAV-
314 818, a biotinylated compound that lacks antiviral activity (PAV-543; structure in Fig. S1), or the DMSO
315 vehicle (Fig. 6A). Quantification of red fluorescent spots, which represent sites where biotinylated
316 compound and Gag are colocalized, revealed 5.5-fold more spots in cells treated with 10 μM PAV-818
317 than in cells treated with an equivalent concentration of the control compound PAV-543, and a slightly
318 greater difference relative to DMSO treated cells (Fig. 6B, C). Moreover, the number of biotin-Gag
319 spots observed with PAV-818 treatment displayed a dose-response relationship (Fig. 6B, C). Controls
320 revealed that only a background level of spots was observed when uninfected 293T cells were treated
321 with PAV-818, as would be expected given that uninfected cells lack Gag (Fig. 6B, C). Additionally, as
322 expected, when antibody to biotin was replaced with a nonimmune control antibody only a few spots
323 were observed; similar results were observed when antibody to Gag was replaced with a nonimmune
324 control (Fig. S2). Together these data provide evidence that PAV-818 colocalizes with Gag in HIV-1
325 infected human cells.

326 **Compound-specific resistance mutations were not observed in *gag* or *pol* after 37 weeks of**
327 **selection with PAV-206**

328 The colocalization of PAV-818 with HIV-1 Gag suggested a straightforward model in which Gag is
329 the target of this assembly inhibitor. If this is the case, then selection for resistance to the compound
330 should result in rapid acquisition of compound-specific mutations in the *gag* gene, analogous to what
331 has been observed for all antiretrovirals that target viral gene products (41). To determine if
332 development of resistance under selection could identify a viral target for this compound, we infected
333 MT-2 T cells and passaged them under selection with PAV-206 for 37 weeks, increasing the drug
334 concentration by two-fold whenever evidence of resistance was observed, and periodically sequencing
335 virus to identify dominant mutations (Fig. 7A, sequencing events indicated by red arrows). We also
336 selected with nelfinavir, a well-studied protease inhibitor, in parallel, as a positive control.

337 As would be expected, we observed that 37 passages in the presence of nelfinavir led to the
338 emergence of three well known resistance mutations in HIV-1 protease: L90M, V77I, and L10F
339 (indicated in red in Fig. 7B using HXB2 genome numbering; Table S1), with L90M being a primary
340 resistance mutation and V77I and L10F being common secondary mutations that further boost nelfinavir
341 resistance (42-46). L90M and V77I were first detected as dominant mutations at passage 29, just before
342 the virus developed a high level of resistance, defined here as replication in a concentration of nelfinavir
343 that is 16-fold higher than the EC50. L10F was detected later, becoming dominant at passage 37. In
344 addition to these well described non-synonymous protease-resistance mutations, two non-synonymous
345 substitutions in Gag emerged during nelfinavir selection (indicated in blue in Fig. 7B; Table S1). These
346 substitutions, A224T and H219Q, are in the cyclophilin A binding loop of Gag and were detectable by
347 passage 21 and 29, respectively. H219Q and other substitutions in the cyclophilin A binding loop
348 (amino acids 217-225 in Gag) are polymorphisms in the Los Alamos Database (47, 48) that are known
349 to modulate incorporation of cyclophilin A into virions when virus is passaged in cyclophilin-A-rich
350 immortalized CD4+T cells even in the absence of drugs, thereby resulting in virion cyclophilin A levels

351 that are optimal for replication in these cell lines (49, 50). From these data, we infer that in the
352 nelfinavir selection group, a tissue-culture-adaptive cyclophilin A binding loop polymorphism initially
353 emerged in Gag and likely led to improved fitness and replication in a drug concentration 8-fold greater
354 than the EC50; this was followed later by nelfinavir-specific resistance mutations, which likely led to
355 high level nelfinavir resistance.

356 Given the results with nelfinavir, we were surprised to find no dominant PAV-206-specific
357 mutations in the *gag* or *pol* genes upon selection with PAV-206 in parallel. Notably, we did detect a
358 dominant drug-independent, tissue-culture adaptive mutation in the cyclophilin A binding loop of Gag in
359 the PAV206 selection, as had been observed with nelfinavir. Specifically, at passage 19, a V218M
360 substitution in the cyclophilin A binding loop (Fig. 7A, B; Table S2). Like the cyclophilin A binding
361 loop substitutions observed with nelfinavir selection, V218M improves viral fitness in cyclophilin-A-
362 rich CD4+ T cells through optimizing cyclophilin binding (47). Unlike with nelfinavir selection, no
363 other dominant non-synonymous mutations were observed in the *gag* or *pol* genes during 37 weeks of
364 selection with PAV-206; moreover, high level resistance was also not observed (Fig. 7A, B), with an
365 unsuccessful passage in a PAV-206 concentration that was 16-fold higher than the EC50 (J. Reed,
366 unpublished observations).

367 While our primary interest was in dominant non-synonymous mutations in *gag* or *pol*, which include
368 the most plausible targets of PAV-206, we also looked for mutations elsewhere in the HIV-1 genome.
369 Interestingly, non-synonymous mutations in *env* were observed in both selection groups (A541V,
370 Q550H, and S144R in the nelfinavir selection group, and N302Y, D547G, and Q550H in the PAV-206
371 selection group in Fig. 7A, B; Table S1, S2). These mutations are known to confer global replication
372 advantage or serve as tissue culture adaptations. Specifically, A541V (observed at nelfinavir passage
373 29) was recently shown to confer broad escape from defects in virus replication caused by either virus
374 mutations or antiretroviral drugs, most likely by increasing cell-to-cell transmission in T cell lines (51).
375 Similarly, N302Y and D547G (observed at PAV-206 passage 27) are thought to increase fusion kinetics

376 (52) and enhance fusogencity (53), respectively, and likely confer global replication advantages.
377 Q550H, which arose during both PAV-206 and nelfinavir selection, has been observed in the absence of
378 drug treatment (54) and is therefore likely to be a tissue culture adaptation. Thus, these *env* mutations
379 are not specific to PAV-206 selection. Finally, we also observed three synonymous mutations arising in
380 *env* upon PAV-206 selection (Table S2). Overall, we concluded from these resistance studies that
381 replication in PAV-206 for 37 weeks failed to select for any PAV-206-specific resistance mutations in
382 *gag* or *pol*, and therefore differed markedly from the nelfinavir selection control, which demonstrated
383 the classic pattern of multiple resistance mutations emerging in the viral target of the drug. Consistent
384 with this conclusion, we observed a high level of resistance in the nelfinavir selection group at passage
385 33 that correlated with emergence of nelfinavir-specific mutations in *pro*, while resistance to PAV-206
386 failed to rise above the moderate level that is likely due to tissue-culture adaptation and mutations that
387 confer global replication advantage in T cells (Fig. 7A).
388

389 **PAV-206 colocalizes with host components of assembly intermediates, suggesting a host-targeting**
390 **mechanism**

391 Our studies to this point had shown that the PAV-206 chemotype colocalizes with Gag *in situ* (Fig.
392 6) and appears to inhibit Gag assembly (Fig. 4), but unexpectedly does not appear to target Gag or
393 GagPol based on resistance studies (Fig. 7). This led us to hypothesize that PAV-206 and its analogs
394 colocalize with host proteins as well as Gag, which would raise the possibility that PAV-206 targets a
395 host protein or viral-host interface that is critical for assembly. This possibility is made more plausible
396 by the fact that these compounds were identified through assembly screens that recapitulate host-
397 catalyzed capsid assembly pathways. In the case of HIV-1 immature capsid assembly, two host
398 proteins, ABCE1 and DDX6, are known to promote assembly and are associated with Gag, serving as
399 markers of Gag-containing assembly intermediates (26, 30-34). Thus, we used PLA to next ask whether
400 PAV-206 colocalizes with these Gag-associated host proteins.

401 293T cells chronically infected with HIV-1 were treated with either the biotinylated antiretroviral
402 PAV-818, or the biotinylated inactive PAV-543, or DMSO and subjected to biotin-ABCE1 PLA (Fig.
403 8A). Quantification of red fluorescent spots representing sites where biotinylated compound and
404 ABCE1 are colocalized *in situ*, revealed 14.3-fold more spots in cells treated with the antiviral PAV-818
405 (10 μM) than in cells treated with an equivalent concentration of PAV-543 and a similar difference
406 relative to DMSO treatment (Fig. 8B, C). Additionally, the number of biotin-ABCE1 spots observed
407 with PAV-818 treatment displayed a dose-response relationship (Fig. 8B, C). Interestingly, PAV-818
408 colocalized with ABCE1 as strongly in uninfected 293T cells as in HIV-1 infected human cells (Fig. 8B,
409 C). As expected, controls in which antibody to biotin or to ABCE1 were individually replaced with a
410 nonimmune control antibody generated very few PLA spots (Fig. S3). PAV-818 was also found to
411 colocalize with DDX6 in chronically HIV-1 infected 293T cells by PLA, with 5.1-fold more spots
412 observed in PAV-818- vs. DMSO-treated cells (Fig. 9A). As a control, we also showed that ABCE1 is
413 colocalized with DDX6 in 293T cells chronically infected with HIV-1, as would be expected from our
414 coimmunoprecipitation studies (30), using PLA with antibodies to DDX6 and ABCE1 (Fig. 9B). Thus,
415 this novel antiretroviral compound colocalizes with HIV-1 Gag and with the host proteins ABCE1, and
416 DDX6, all of which are components of HIV-1 assembly intermediates.
417
418
419
420
421
422
423
424
425

426 **DISCUSSION**

427 Here we report our discovery of a family of small molecules, PAV-206 and its analogs, that potently
428 inhibit HIV-1 replication by acting on intracellular viral late events, a stage of the viral life cycle that is
429 not specifically targeted by potent inhibitors currently in use or reported to be in development.
430 Importantly, the exact target and mechanism of action of this compound remain to be determined;
431 however, the data from virologic, resistance, and imaging studies presented here raise the intriguing
432 possibility that this compound does not target a viral protein, but instead may target a host component of
433 a multi-protein complex that plays an important role in assembly of the immature HIV-1 capsid (Fig.
434 10). While further studies will be needed to test this hypothesis, PAV-206 and its analogs should be of
435 great interest even at this early stage given that all antiretroviral drugs in use except one (CCR5
436 antagonists) target viral proteins and that host-targeting antivirals offer a high genetic barrier to
437 resistance that will be key as resistance to existing drugs becomes more prevalent (55, 56).

438 Most exciting in this regard was our observation that after selection with increasing concentrations
439 of PAV-206 for 37 weeks in MT-2 T cells, sequence of replicating virus revealed no compound-specific
440 mutations in *gag* or *pol* (Fig. 7), suggesting that PAV-206 acts by a mechanism that is independent of
441 direct targeting of Gag. Additionally, high level resistance to PAV-206 was not observed during this
442 time (Fig. 7). Such behavior is distinctly unusual, since all existing classes of direct-acting antiretroviral
443 drugs result in rapid development of resistance mutations in their viral targets upon single drug
444 treatment (41). The unusual nature of this finding was emphasized by our contrasting finding that 37-
445 week selection with the protease inhibitor nelfinavir in parallel did result in three known resistance
446 mutations in the HIV-1 protease as well as high-level resistance (allowing growth in drug concentrations
447 16X higher than the EC50), as would be expected.

448 We did observe two other categories of mutations during both PAV-206 and nelfinavir selection.
449 The first are known tissue-culture adaptations (Fig. 7; Table S1 and S2). Most of these were in the
450 cyclophilin A loop of Gag and are known to reduce the amount of cyclophilin A incorporated into

451 virions during passage in cyclophilin A-rich immortalized CD4+ T cells, in the presence or absence of
452 antiretroviral drugs (49, 50). One known tissue culture adaptation (54) was observed in *env* (Q550H)
453 and arose in both selection groups. Mutations in a second category were also not compound-specific,
454 and likely confer global replication advantage, as best demonstrated for A541V (51). The emergence of
455 the earliest of these various compound-independent mutations, the cyclophilin A binding loop
456 polymorphism V218M, as a subdominant mutation might explain the modest resistance observed in the
457 PAV-206 selection experiment (allowing virus replication in a PAV-206 concentration 8X higher than
458 the EC50). In support of this possibility, the appearance of modest resistance (to 8X EC50) in the
459 nelfinavir selection control by passage 20 correlated with emergence of a cyclophilin A binding loop
460 polymorphism and preceded the time when the drug-specific protease mutations became dominant.
461 Further studies will be needed to test the hypothesis that these mutations allow low level replication in
462 the presence of compound.

463 While additional studies will be required to identify the target of PAV-206, the surprising lack of
464 compound-specific viral resistance mutations in *gag* or *pol* raises the possibility that this compound acts
465 on a host protein. Two other observations are consistent with that hypothesis. First, this compound was
466 identified using novel screens that recapitulate host-catalyzed pathways in which assembling capsid
467 proteins form a series of host-protein containing assembly intermediates, culminating in formation of the
468 completed immature capsid. Such an assembly pathway screen was previously shown to identify a host-
469 targeting small molecule that potently inhibits RABV in cell culture (35). Second, our imaging studies
470 show that PAV-206 colocalizes with Gag as well as ABCE1 and DDX6 (Figs. 6, 8, 9), two host
471 enzymes known to be associated with Gag in assembly intermediates as shown by PLA and
472 coimmunoprecipitation (24-27, 30, 32-34); here, we additionally showed that ABCE1 colocalizes with
473 DDX6 by PLA (Fig. 9), consistent with previous co-immunoprecipitation results (30). Interestingly, our
474 studies found that PAV-206 colocalizes with at least one of these host enzymes (ABCE1) in the absence
475 of HIV-1 infection (Fig. 8), suggesting that the compound acts on the host RNA-granule-related RNP

476 complex that is the precursor of assembly intermediates, even in the absence of Gag. Additional studies
477 will be required to identify the direct target of this chemotype through crosslinking approaches that
478 utilize the diazirine group in PAV-818, but based on data presented here, we hypothesize that the target
479 may be a component of the host-RNP-complex-derived assembly intermediates.

480 PAV-206 and its analogs are also of great interest because, to our knowledge, they are the first
481 potent small molecules shown to selectively inhibit late events in the HIV-1 life cycle. Unlike
482 previously reported compounds that target CA with high potency (i.e. EC50 in the nM range or below,
483 e.g. (12, 17, 57-59)) the chemotype reported here has no effects on viral early events and acts entirely on
484 late events (Fig. 3). Moreover, PAV-117 dramatically reduces virus production (Figs. 3, 4), indicating
485 that it acts on intracellular late events. PAV-117 treatment of infected cells did not reduce steady-state
486 levels of two cellular proteins suggesting that PAV-117 does not globally inhibit protein synthesis as
487 would be expected based on the screening strategy. PAV-117 treatment did lead to a modest reduction
488 in steady-state Gag levels, although it is unlikely this modest reduction in steady-state Gag explains the
489 reduction in virus production. Although we cannot rule out the possibility that the modest reductions in
490 steady-state Gag levels are due to PAV-117 specifically inhibiting Gag synthesis, we favor the
491 hypothesis that the reduced Gag levels are due to degradation of assembly intermediates that are
492 associated with compound. Consistent with this hypothesis we do observe a reduction in the steady-
493 state levels of the final (~500S) assembly intermediate (Fig. 4). Nevertheless, additional studies will be
494 needed to determine the exact mechanism of action of PAV-206 and its analogs.

495 Finally, it should be noted that discovery of these compounds constitutes a compelling validation of
496 the importance of HIV-1 RNA-granule-related assembly intermediates in virus production.
497 Surprisingly, the existence of assembly intermediates containing RNA granule proteins continues to be
498 questioned, even though numerous groups in addition to ours have implicated RNA granule proteins as
499 being important for assembly of diverse retroviruses and retroelements. For example, knockout studies
500 by the Sandmeyer group demonstrated that RNA granule proteins are required for Ty3 retrotransposition

501 in yeast and likely act during assembly (60-62). Additionally the Linial group found that the RNA
502 granule protein DDX6 is required for foamy virus packaging (63), and the Mouland group has shown
503 that the RNA granule protein Stau1 plays an important role in HIV-1 Gag assembly and packaging (64-
504 67). Finally, the Kewalramani and Pathak groups have demonstrated that the RNA granule protein
505 MOV10 influences immature HIV-1 assembly (68, 69). Data presented here shows that the study of
506 host-derived RNA-granule-derived HIV-1 assembly intermediates has led to discovery of the first
507 compounds that specifically inhibit intracellular HIV-1 late events. Thus, these data add strong support
508 to the view that such assembly intermediates not only exist but are highly relevant to our understanding
509 of HIV-1 assembly as well as development of antiretroviral compounds for treatment of multidrug
510 resistant HIV-1 in the future.
511
512
513
514
515
516
517
518
519
520
521
522
523
524
525

526 **METHODS**

527 **Plasmids and proviral constructs.**

528 In this study several variants of the HIV-1 NL4-3 proviral clone were utilized. For infection of PBMC,
529 we utilized the NL4-3 Infectious Molecular Clone (pNL4-3) from Dr. Malcolm Martin obtained through
530 the NIH AIDS Reagent Program, Division of AIDS, NIAID, NIH (Catalog Number 114; (70)). For
531 infection of MT-2, the pNL4-3 plasmid was modified to express *Renilla* luciferase in place of *nef* to
532 make the HIV-1 pNL4-3 RLuc plasmid. For single round MT-2 cell infections used to assay only HIV-
533 1 early events, we introduced an *env* deletion (KpnI-BglII) into the RLuc plasmid to make pNL4-3 RLuc
534 Δ*env*. We also used several variants of the HIV-1 LAI proviral clone. Chronically infected H9 and
535 293T cells were generated using HIV-1 pLAI *vpr*- *nef*- *puro*+, a proviral plasmid that contains a
536 puromycin gene in place of *nef* for selection and two stop codons introduced into the NcoI site within
537 *vpr* to inactivate Vpr (71). For single round MT-2 cell infections used to evaluate viral late events, we
538 used pLAI *pro*- Δ*env* which we have described previously (30). The plasmid pcDNA NL4-3 Env used
539 for pseudotyping was generated by cloning a Geneblock DNA fragment of codon-optimized NL4-3 *env*
540 (Integrated DNA Technologies ((IDT), Coralville, IA) into a pcDNA vector by Gibson assembly (72).
541 For infection of SupT1.CCR5 cells, we utilized a molecular clone of a subtype A primary isolate, Q23-
542 17(73), that was modified to express a subtype A BG505 *env* (74, 75) and was obtained from Julie
543 Overbaugh. Infection of G355-5 cells with FIV utilized the FIV-34TF10 ORFA+ proviral clone,
544 described previously (31). The psPAX2 Gag-Pol helper plasmid was obtained from Didier Trono via
545 Addgene (plasmid # 12260; http://n2t.net/addgene:12260). To evaluate compound activity against
546 FLUV, plasmids required for production of FLUV A/WSN/33 (76) were obtained from Andrew Pekosz.
547

548 **Cells and transfection.** The feline astrocyte cell line G355-5 was obtained from ATCC (Manassas,
549 VA; CRL-2033) and maintained in McCoy 5A (modified) medium supplemented with 10% fetal bovine
550 serum (complete McCoy 5A). G355-5 cells were transfected with 1 to 6 µg DNA in 6 cm dishes using

551 X-treameGENE 9 (Roche, Basel, Switzerland). The 293T/17 cell line was obtained from ATCC (CRL-
552 11268) and maintained in DMEM media supplemented with 10% fetal bovine serum and 1% penicillin-
553 streptomycin (complete DMEM). 293T cells were transfected with 1 mg/mL polyethylenimine (PEI;
554 Polysciences, Warrington, PA) at a ratio of PEI-to-DNA of 3:1. The MT-2 cell line was obtained from
555 Dr. Douglas Richman through the NIH AIDS Reagent Program, Division of AIDS, NIAID, NIH
556 (Catalog Number 237; (77, 78)). SupT1.CCR5 cells, a SupT1 cell line stably expressing CCR5 HIV-1
557 coreceptor (79), , were obtained from Julie Overbaugh. MT-2 and SupT1.CCR5 cells were maintained
558 in RPMI supplemented with 10% fetal bovine serum and 1% penicillin-streptomycin (complete RPMI).
559 TZM-bl cells were obtained from Dr. John C. Kappes, and Dr. Xiaoyun Wu through the NIH AIDS
560 Reagent Program, Division of AIDS, NIAID, NIH (Catalog number 8129; (80-84)). The MDCK.2 cell
561 line was obtained from ATCC (CRL-2986) and were maintained in MEM media supplemented with
562 10% fetal bovine serum, 1% penicillin-streptomycin, 1% non-essential amino acids solution, and 1%
563 sodium pyruvate (complete MEM).
564
565 **HIV-1 chronically infected cell lines.** The 293T-HIV and H9-HIV lines stably express the provirus
566 LAI *vpr- nef- puro+*. These lines were generated by infecting either 293T/17 or H9 cells with NL4-3
567 *vpr- nef- puro+* at an MOI of 1, followed by selection with and maintenance in complete media
568 supplemented with 0.5 μg/mL puromycin.
569
570 **Antibodies for western blotting and proximity ligation assay.** To detect HIV-1 Gag p24 in cell
571 lysates and virus pellets by WB, we used αGag p24 mouse IgG_1 monoclonal antibody isolated from the
572 hybridoma 183-H12-5C obtained from Bruce Chesebro through the AIDS Reagent Program Division of
573 AIDS, NIAID, NIH (catalog number 1513; (85)). Commercial antibodies were used to detect GAPDH
574 (Abcam, Cambridge, MA; ab9485) and actin (Millipore-Sigma, St Louis, MO; A2066) in cell lysates by
575 WB. Isotype specific secondary antibodies utilized for WB were obtained from Bethyl Laboratories

576 (Montgomery, TX). For proximity ligation assay (PLA) we utilized the αGag antibody described for
577 WB above, αbiotin rabbit IgG (Bethyl Laboratories, A150-109A), affinity purified αABCE1 rabbit IgG
578 which we have previously described (34), αbiotin mouse IgG (Jackson Immunoresearch Labs, West
579 Grove, PA,; 200-002-211), αDDX6 mouse IgG (Millipore-Sigma; WH0001656M1),
580 and αDDX6 rabbit IgG (Bethyl Laboratories; A300-461A). Rabbit IgG (Millipore-Sigma; I5006) and
581 mouse IgG (Millipore-Sigma; I5381) was used for PLA nonimmune controls.
582
583 **Virus infectivity measurement.** Infectivity was measured by titering stocks on TZM-bl cells. Cells
584 seeded 7500 cells/well into 96-well polystyrene tissue culture plates were infected 24h later with
585 dilutions of culture supernatant or virus stock containing 20 µg/ml DEAE dextran in a 50 µL volume for
586 4 h at 37°C. After infection, 150 µL of complete DMEM was added and plates were incubated at 37°C
587 for 48 h. Cells were fixed with 1% formaldehyde/0.2% glutaraldehyde/PBS for 5 min and washed with
588 PBS. To determine infectious units, cells were incubated with 50 µL of X-Gal stain (4 mM potassium
589 ferrocyanide, 4 mM potassium ferricyanide, 2 mM $MgCl_2$, 0.4 mg/mL 5-Bromo-4-Chloro-3-Indolyl β-
590 D-Galactopyranoside prepared in PBS) for 50 min at 37°C. Following staining cells were washed
591 several times with PBS and blue cells (only wells with < 100 cells) were counted to determine infectious
592 units (IU) per mL. To determine relative infectivity, cells were seeded, infected, fixed, and washed as
593 above, but instead of X-Gal stain, 100 µL of MUG stain (200 µg/mL 4-methylumbelliferone β-D-
594 galactopyranoside prepared in DMEM) was added and incubated at 37°C for 25 min. After incubation,
595 the reaction was terminated with 100 µL of 1M Na_2CO_3 and well fluorescence determined using 360 nm
596 and 449 nm for excitation and emission settings, respectively (Synergy H1; BioTek Instruments, Inc.,
597 Winooski, VT, USA). The relative fluorescence was used to compare infectivity between samples.
598
599 **PBMC activation.** Thawed, unstimulated PBMC cells (BenTech, Seattle, WA) were pelleted by
600 centrifugation 228 x g for 8 min in an Allegra centrifuge (Beckman, Brea, CA). Pellets were

601 resuspended in activation medium containing RPMI supplemented with 21 ng/mL human IL-2
602 (Peprotech, Rocky Hill, NJ; #200-02), 1.5 µg/mL PHA (Remel, San Diego, CA; R30852801), 10% fetal
603 bovine serum, and 1% penicillin-streptomycin, at a density of $2x10^6$ cells/mL. After a three-day
604 incubation, cells were collected and resuspended in RPMI with 20% FBS and 10% DMSO, and frozen
605 as $50x10^6$ cells per vial.
606
607 **HIV-1 virus production.** To produce HIV-1 viral stocks 293T/17 cells were seeded at $10x10^6$ cells in a
608 T175 flask, transfected for 24 h, washed, and incubated in complete DMEM. Media from 48 and 72 h
609 post transfection collections was pooled, filtered with a 0.45 µm PES membrane, and 0.5 mL aliquots
610 were stored at -80°C. To produce viral stocks of NL4-3, Q23.BG505 and LAI *vpr- nef- puro*+, 36 µg of
611 proviral plasmids were used per T175 flask. To produce viral stocks of NL4-3 RLuc Δ*env* pseudotyped
612 with NL4-3 Env, 36 µg of the proviral plasmid, and 12 µg of pcDNA NL4-3 Env were co-transfected.
613 To produce viral stocks of LAI pro- Δ*env* pseudotyped with NL4-3 Env, 27 µg of proviral plasmid, 15
614 µg of pcDNA NL4-3 Env, and 18 µg of psPAX2 (Gag-Pol helper plasmid) were co-transfected.
615
616 **FLUV virus production.** FLUV A/WSN/33 viral stocks were prepared in MDCK.2 cells as described
617 previously (86).
618
619 **FIV virus production and RT assay.** G355-5 cells were transfected in 6-well plates and each well was
620 transfected with 2 µg per well of FIV 34TF10 ORFA+ proviral plasmid. At 24 h post transfection, cells
621 were washed and media replaced with 4 ml of complete McCoy 5A. At 144 h post transfection, media
622 was filtered with a 0.45 µm syringe filter, aliquoted, and stored at -80C. Reverse transcriptase activity
623 in media from FIV or mock-transfected cells was estimated using SG-PERT (87). A set of recombinant
624 RT standards (EMD Millipore, Molsheim, France; catalog# 382129) ranging from 5.12e3 nU/mL to
625 5.12e9 nU/mL was used to estimate the nU/mL of reverse transcriptase activity in the FIV stock.

626 **Inhibition of HIV-1 replication.**

627 *MT-2 spreading infection assay.* Inhibition of HIV-1 viral replication was assayed in a spreading
628 infection using MT-2 cells and NL4-3 RLuc reporter virus. For dose-response curves, compounds were
629 initially diluted with DMSO to 100-times the starting concentration in a 96-well plate and subjected to a
630 series of 3-fold dilutions in DMSO for a total of eight or nine dilutions. If a single compound
631 concentration was tested, the compound was diluted to 100-times the desired concentration in DMSO.
632 Compounds were then diluted 50-fold with infection media prepared by diluting NL4-3 RLuc virus
633 stock to 400 IU/100 µL with complete RPMI. Then 100 µL of 50-fold diluted compound was
634 transferred to 20,000 MT-2 cells that were pre-seeded in 96-well plates in 100 uL complete RPMI for a
635 final volume of 200 u, followed by incubation at 37°C for 96 h. The final MOI in infected plates was
636 0.02 and the final DMSO concentration in all wells was 1%. All assays were run with three replicates.
637 For each replicate, one well received DMSO only and one well received media only for normalization
638 and background correction. To assay inhibition of HIV-1 replication, 100 µL of media was removed
639 and discarded and 10 µL of 15 µM EnduRen luciferase substrate was added to each well, followed by
640 incubation for 1.5 h at 37°C. Plates were read on a luminescence plate reader (Synergy H1; BioTek
641 Instruments, Inc.).

642 *SupT1.CCR5 spreading infection* assay. The SupT1.CCR5 assay was as described for the MT-2
643 spreading infection assay, with the following exceptions: 12.5 uL of Q23.BG505 virus stock was used
644 per well, and inhibition of HIV-1 replication was determined by measuring the relative infectivity
645 produced form infected cells using the MUG assay (see virus infectivity measurements above).

646 *PBMC spreading infection* assay. The PBMC assay was as described for the MT-2 spreading
647 infection assay with the following exceptions. Frozen activated PBMC cells were thawed and
648 resuspended in complete PBMC media containing RPMI supplemented with 21 ng/mL human IL-2
649 (Peprotech; #200-02), 10% fetal bovine serum and 1% penicillin-streptomycin, at $0.5x10^6$ cells/mL for 3
650 days in 37°C tissue culture incubator. Cells were collected and adjusted to $2x10^6$ cells/mL in complete

651 PBMC media and bulk infected for 2 h with NL4-3 virus stock at a MOI of 0.008 at 37°C. Compound
652 dilutions were prepared in complete PBMC media as above, but without virus, and 100 uL of diluted
653 compound was transferred to 96-well U-bottom plates. Bulk infected cells were pelleted and
654 resuspended in complete PBMC media at $1x10^6$ cells/mL and 100 μL of cell suspension was transferred
655 to each well at 100,000 cells per well with diluted compound. After 96 h, media was collected for
656 relative infectivity measurements as with the SupT1.CCR5 spreading infection assay.
657
658 **FIV inhibition assay.** Inhibition of FIV spreading infection was assayed using G355-5 cells, seeded on
659 the prior day at 8000 cells/well in a 96-well plate. Preparation and addition of compounds were as in the
660 MT-2 spreading infection assay with the following differences: for infection, 1954 nU RT activity of
661 the FIV-34TF10 ORFA+ stock was used per well, infection assays proceeded for 144 h, and infectious
662 virus production was measured using the SG-PERT assay described above.
663
664 **Virus pelleting.** For Fig. 3B, culture supernatants were collected at 48 h and virus was pelleted by
665 adding 75 μL of 17% PEG 6000/0.8M NaCl/PBS to 75 μL media from the assay in a 96-well V-bottom
666 polypropylene plate. PEG and media were incubated on ice for 2 h or overnight at 4°C. Virus was
667 pelleted at 1847 x g for 30 min at 4°C in the plate in an Allegra centrifuge (Beckman) and the pellet was
668 resuspended in 50 uL of loading buffer with DTT for analysis by WB with αGag. For Fig. 4, culture
669 supernatants were collected 48 h post infection and filtered through a 0.45 μm PES syringe filter to
670 remove any remaining cells. Virus-like particles were centrifuged through a 30% w/v sucrose/PBS
671 cushion at 130,000 x g, 30 min, 4°C in an SW55Ti rotor (Beckman), and the virus pellet harvested for
672 analysis by WB with αGag.
673

674 **MT-2 acute infection assay.** MT-2 cells were diluted to $2x10^6$ cells/mL with complete RPMI and bulk
675 infected at a MOI of 1 for 2 h at 37°C. Compound was diluted to 100-times the final required
676 concentration with DMSO. The compound dilutions and DMSO only controls were then further diluted
677 50-fold with complete RPMI, and 1 mL of the dilutions was added per well in a 12-well plate. Bulk
678 infected cells were then washed and adjusted to $0.5x10^6$ cells/mL, and 1 mL of infected cells was added
679 to each well containing diluted compound or DMSO. At 48h, media was collected for virus pelleting as
680 described above and cells were washed and lysed (see cell lysis below).
681
682 **Cell lysis.** MT-2 cells were collected and washed three times by pelleting at 200 x g for 5 min at 4°C in
683 an Allegra centrifuge (Beckman) and resuspending cells in ice-cold PBS. Cell pellets were lysed with
684 250 µL lysis buffer (20 mM HEPES pH 7.9, 14 mM KAc, 1 mM $MgCl_2$, 0.3% NP40) followed by
685 shearing 20-times with a 20-gauge needle. Cell lysate was then clarified 200 x g for 10 min at 4°C in an
686 Allegra centrifuge (Beckman). Supernatant was transferred to a fresh tube and further clarified by
687 centrifugation at 18,000 x g for 10 min at 4°C in a microfuge (Beckman), and supernatant transferred to
688 a fresh tube.
689
690 **Velocity sedimentation.** To prepare gradients, 10%, 15%, 40%, 50%, 60%, 70%, and 80% w/v sucrose
691 solutions were prepared with water and then each was diluted 1/10 with a 10x stock of the lysis buffer
692 used to harvest cells (see cell lysis). For each gradient, ~100 µL of cell lysate (~100 µg of total protein)
693 was layered on a 5-ml step gradient containing equivalent layers of each diluted sucrose solution
694 prepared and subjected to velocity sedimentation in a Beckman MLS-50 rotor 217,000 x g for 45 min at
695 4°C. Gradients were fractionated from top to bottom, and pelleted material was harvested for WB.
696 Aliquots of fractions and pellet were analyzed by SDS-PAGE, followed by WB with αGag. Gag in
697 pellet, which likely represents denatured Gag, was not included in the quantification of the velocity
698 sedimentation gradients and represented less than 10% of total Gag signal in the gradient. The method

699 for estimating the migration of particles with different S values in gradients has been described
700 previously (28).
701
702 **Inhibition of HIV-1 early events.** For Fig. 3A, the assay described under MT-2 spreading infection
703 assay was used with the following exceptions: MT-2 cells were infected with 0.5 μL/well of HIV-1
704 NL4-3 RLuc Δ*env* virus pseudotyped with NL4-3 Env and luciferase was measured at 48 h instead of 96
705 h.
706
707 **Inhibition of HIV-1 late events.** For these experiments, we used H9-HIV, a chronically infected H9 T
708 cell line. Compounds were diluted as described under MT-2 spreading infection above. To measure
709 inhibition of infectious virus production (Fig. 3B, black graph), media were collected and relative
710 infectivity of virus in the media was measured using the MUG assay (see virus infectivity measurements
711 above). To measure inhibition of virus production (Fig. 3B, blue graph and blot), PEG pelleted virus
712 (harvested as described in virus pelleting above) was analyzed by WB with αGag.
713
714 **FLUV antiviral assay.** Inhibition of FLUV replication was assayed using infection of MDCK.2 cells.
715 A day before the assay, MDCK.2 cells were seeded at 30,000 cells/well in complete MEM in a 96-well
716 plate. The next day, seeded cells are washed with PBS and incubated for 1 h with 100 μL of FLUV
717 A/WSN/33 stock diluted in VGM media containing 42 mM HEPES, 0.125% BSA, and 1 μg/mL TPCK-
718 trypsin (final MOI of 0.001). Cells were then washed with PBS and incubated in 90 uL of complete
719 MEM. Single compound dilutions were prepared in complete MEM at 10x the desired final
720 concentration, and 10 μL of DMSO or 10x compound was added to infected cells for final volume of
721 100 μL. At 24 h post infection, media was aspirated, cells were washed with PBS, and 100 μL of
722 complete MEM was added to each well. After a 2 h incubation, media were collected for TCID50
723 determination.

724 **FLUV TCID50 assay.** FLUV TCID50 was assessed on MDCK.2 cells. MDCK.2 cells were seeded at
725 30,000 cells/well in complete MEM in a 96-well plate and the next day the complete MEM was
726 exchanged for 100 µL VGM media (as in the FLUV antiviral assay). Ten-fold serial dilutions of virus-
727 containing supernatant were prepared and seven replicates of 11.1 µL of neat and diluted stocks were
728 added to the MDCK cells (final dilutions in the TCID50 plate ranged from 10^{-1} – 10^{-6}). Plates were
729 incubated at 37°C for 3 days, and the number of infected wells in the seven replicates for each dilution
730 was determined by visual inspection. These data were used to calculate TCID50/mL using the Reed and
731 Muench method (88).
732
733 **Cytotoxicity Assays**. For each viral inhibition assay, a cytotoxicity assay was performed in parallel on
734 uninfected cells by adding 1/10th volume of AlamarBlue (Thermo Fisher, Waltham, MA; DAL1199) to
735 the plates and mixing well. AlamarBlue-treated plates were incubated for 2-3 h at 37°C (timing was
736 optimized for linear signal), mixed well, and read using a fluorescence plate reader with 560 nm and 590
737 nm as excitation and emission settings, respectively (Synergy H1; BioTek Instruments, Inc.).
738
739 **Resistance Assay.** Resistance selections were carried out in 12-well tissue culture plates. First,
740 compound dilutions were prepared by adding 1.25 mL of complete RPMI to each well followed by 25
741 µL of compound that was diluted to 100x the desired final concentration in DMSO. For the first
742 passage, NL4-3 virus stock was then added to achieve a MOI of 0.01. For subsequent passages, 150 µL
743 of the previous passage was added instead. Finally, 0.2×10^6 MT-2 cells were added in 1.25 mL of
744 complete RPMI. The cultures were incubated at 37°C until they reach maximum viral CPE, as
745 determined by visual inspection for the formation of syncytia (3-7 days). Selection was begun at
746 1x[EC50] and then increased 2-fold whenever maximum CPE was achieved in a time frame similar to
747 that achieved by virus passaged in DMSO. At the end of each selection cells were pelleted from the
748 media by centrifugation 200 x g for 5 min in an Allegra centrifuge (Beckman) and supernatant was

749 transferred for storage at -80C. PAV-206 and nelfinavir selections were carried out in parallel for 37
750 weeks.
751
752 **Sequencing virus from resistance selection.** Passaged media was first titered on TZM-bl cells and
753 infectious units/ mL determined by X-Gal staining (see Virus infectivity measurement above. Passaged
754 virus was then used to infect MT-2 cells at a MOI of 1 in complete RPMI supplemented with 100 ug/mL
755 DEAE dextran for 3 h at 37°C. Cells were pelleted at 200 x g 5 min in Allegra centrifuge (Beckman)
756 and then resuspended in complete RPMI. At 15 hours post infection, cells were washed three times with
757 ice-cold PBS and then viral cDNA from the cell pellet was harvested using a Spin Miniprep kit (Qiagen,
758 Venlo, Netherlands). Viral cDNA was amplified by PCR using the Herculase II polymerase (Agilent,
759 Santa Clara, CA) and amplified viral cDNA was gel purified using a Spin Gel Purification kit (Qiagen).
760 Two sets of primers were used to amplify viral cDNA in two overlapping fragments. The first half of
761 the genome from 132 base pairs before the start of *gag* to midway through *vpr* was amplified with the
762 forward primer 5'-AAGCGAAAGTAAAGCCAGAGG -3' and reverse primer 5'-
763 AACGCCTATTCTGCTATGTCG-3'. The second half of the genome from *vpr* to 252 base pairs into
764 *nef* was amplified with the forward primer 5'-CAGAGGACAGATGGAACAAGC-3' and the reverse
765 primer 5'AGCTGCCTTGTAAGTCATTGG-3'. The LTRs were not sequenced. Gel purified PCR
766 products were then subjected to Sanger sequencing. Gel chromatograms were visually inspected to
767 identify a second chromatogram peak that was equal or larger in height than the peak corresponding to
768 the reference sequence (defined as a ≥ 50% mutation; see Table S1 and S2) or a single chromatogram
769 peak that differs from the reference sequence (defined as a dominant mutation; see Table S1 and S2).
770
771 **Proximity Ligation Assay (PLA).** For each treatment, one-half of a Grace Biolabs Culture Well
772 silicone chamber (Millipore-Sigma; GBL103380) was attached to a cover glass (Carl Zeiss,
773 Oberkochen, Germany; #474030-9000-000) to create four chambers on the cover glass. Each

774 chambered cover glass was placed into a well of a 6-well plate and chambers were coated with poly-L-
775 lysine and allowed to dry overnight. The next day ~$4x10^3$ 293T/17 or 293T-HIV cells were seeded into
776 each chamber and incubated at 37°C for 5-6 h. After cells adhered, they were treated with compound or
777 DMSO. At 16 h post treatment, cells were fixed for 15 min in 4% paraformaldehyde in PBS pH 7.4,
778 permeabilized in 0.5% w/v Saponin in PBS, pH 7.4 for 10 min, and blocked in Duolink blocking
779 solution (Millipore-Sigma) at 37°C for 30 min. Cells were incubated in primary antibodies using the
780 following concentrations: for the Gag-Biotin PLA, mouse αGag p24 was used at 0.2 ug/mL and rabbit
781 αbiotin was used at 4 ug/mL; for the ABCE1-Biotin PLA, rabbit αABCE1 was used at 0.3 ug/mL and
782 mouse αbiotin was used at 0.7 ug/mL; for the DDX6-Biotin PLA, rabbit αDDX6 was used at 1 ug/mL
783 and mouse αbiotin was used at 0.7 ug/mL; for the ABCE1-DDX6 PLA, rabbit αABCE1 was used at 0.3
784 ug/mL and mouse αDDX6 was used at 0.3 ug/mL. For the nonimmune (NI) control PLA experiments,
785 NI control antibodies from the relevant species were used at the same concentration as the primary
786 antibody they replaced. Primary incubation was followed by incubation with Duolink reagents
787 (Millipore-Sigma): oligo-linked secondary antibody, ligation mix, and red amplification/detection mix,
788 with washes in between, as per the Duolink protocol. For concurrent immunofluorescence (IF)
789 following the final 1x PLA Buffer B washes, cells were incubated for 30 min at RT with 1:1000
790 Alexafluor 488 anti-mouse secondary antibody. Cover glasses were mounted using Duolink In Situ
791 Mounting Media with DAPI (Millipore-Sigma), sealed to the glass slides with clear nail polish, allowed
792 to dry for 24 h at RT, and stored at -20°C. Imaging was performed with a Zeiss Axio Observer.Z1/7
793 deconvolution microscope using Zeiss Plan-Apochromat 63X/ aperture 1.4 objective with oil
794 immersion, with Zen 2.6 (blue edition) software. For quantification, five to ten fields, each containing at
795 least three IF-positive cells, were chosen at random and imaged using identical exposure times for each
796 channel (100 milliseconds for the PLA channel in red; 0.5-1 second for the IF channel in green,
797 depending on IF primary antibody; and 20 milliseconds for the DAPI channel in blue). Images were
798 captured as a Z-stack of 80-90 0.24-µm slices that included the entire cell body and 5 µm above and

799 below the cell (~20 µm total). To determine the number of PLA spots per cell, image stacks were
800 processed as follows in FIJI (89). First, an in-focus slice from the IF channel was selected using the
801 Find Focused Slices plugin within ImageJ (Tseng, Q (2020), available from
802 https://sites.google.com/site/qingzongtseng/find-focus) and thresholding was used to generate regions of
803 interest (ROI) that contained only cells. The ROIs identified in the IF channel were applied to a
804 maximum intensity Z-projection of the PLA channel and PLA spots within the ROI were counted using
805 the find maxima function in Fiji, with noise threshold optimized to identify only PLA spots. Nuclei
806 from each field were counted manually to determine the number of cells. Total PLA spots counted were
807 divided by total nuclei to obtain the average number of PLA spots per cell, and these results were plotted
808 with error bars representing SEM, with *n* being the total number of cells counted. The number of fields
809 and cells analyzed for each PLA were: Gag-biotin PLA (Fig. 6) 20 fields, containing a total of 186 - 316
810 cells; ABCE1-biotin PLA (Fig. 8) 10 fields, containing a total of 104 - 155 cells; DDX6-biotin PLA
811 (Fig. 9) 5 fields, containing a total of 60 - 73 cells; DDX6-ABCE1 PLA (Fig. 9) 10 fields, containing a
812 total of 121 cells; Gag-biotin PLA (Fig. S2) 20 fields, containing a total of 213 - 304 cells; rabbit biotin-
813 mouse NI PLA (Fig. S2) 10 fields, containing a total of 107 - 118 cells; rabbit NI-mouse Gag PLA (Fig.
814 S2) 10 fields, containing a total of 131 cells; ABCE1-biotin PLA (Fig. S3) 5 fields, containing a total of
815 53-66 cells; mouse biotin-rabbit NI PLA (Fig. S3) 5 fields, containing a total of 51 - 59 cells; mouse NI-
816 rabbit ABCE1 (Fig. S3) 5 fields, containing a total of 44 - 77 cells. For presentation of images in
817 figures, a central slice of the image stack was chosen, and a region of the field of 1875 pixels x 938
818 pixels was selected and adjusted as follows. For all channels, background was removed by setting the
819 intensity minimum above the background signal. For the PLA channel, the gain on PLA spots was
820 increased for visualization by setting the channel intensity maximum to approximately one-third the
821 intensity of the most intense pixel in the selected field. For the IF channel, IF signal was reduced to
822 improve PLA spot visualization by setting the channel intensity maximum to approximately twice the
823 intensity of the most intense pixel in the selected field. A gray scale image of the PLA channel only and

824 an RGB image of the merged channels (PLA, red; IF, green; and DAPI, blue) were generated and
825 imported into Inkscape, an open source vector graphics editor, to create the final figure layout without
826 further adjustment.
827
828 **Statistical Analysis.** EC50 and CC50 values were determined in Excel using four-parameter logistic
829 regression analysis of dose-response data generated from the viral inhibition or cytotoxicity assays,
830 respectively. Solid-lines on dose-response plots represent the fitted logistic regression. Average EC50
831 and CC50 values were calculated using the geometric mean and average values were reported with the
832 geometric standard deviation (GSD). The statistical difference between pairs of treatment groups in the
833 PLA experiments was analyzed in Excel using a two-tailed unpaired Students *t* test assuming unequal
834 variance.
835
836 **Synthesis of compounds.** See Supplementary Methods.
837
838
839
840
841
842
843
844
845
846
847
848

849 **ACKNOWLEDGMENTS**

850 The following reagents were obtained through the NIH AIDS Reagent Program, Division of AIDS,
851 NIAID, NIH: αGag, p24 mouse IgG_1 monoclonal antibody isolated from the hybridoma 183-H12-5C
852 obtained from Bruce Chesebro (catalog number 1513); HIV-1 NL4-3 Infectious Molecular Clone
853 (pNL4-3) from Malcolm Martin (Catalog Number 114); MT-2 cell line from Douglas Richman (Catalog
854 Number 237); and TZM-bl cells from John C. Kappes and. Xiaoyun Wu (Catalog number 8129). HIV-1
855 Q23.BG505 virus and SupT1.CCR5 cells were obtained from Dr. Julie Overbaugh. The psPAX2 Gag-
856 Pol helper plasmid was obtained from Didier Trono via Addgene (plasmid # 12260). Plasmids for
857 production of FLUV A/WSN/33 were obtained from Andrew Pekosz.

858 We acknowledge Michael Emerman for advice and input.

859 Jaisri Lingappa is a cofounder of Prosetta Biosciences and Jonathan Reed is a consultant for
860 Prosetta Biosciences. Vishwanath Lingappa is a cofounder, CEO, and CTO of Prosetta Biosciences.

861 These studies were funded by NIH R01AI150457, NIH R56 AI145498, and Prosetta Biosciences.
862 Neither of the funders (NIH or Prosetta Biosciences) had any role in study design, data collection and
863 interpretation, or the decision to submit the work for publication.

864

865

866

867

868

869

870

871

872

873

874 **REFERENCES**

875 1. Abner E, Jordan A. 2019. HIV "shock and kill" therapy: In need of revision. Antiviral Res
876 166:19-34.
877 2. Pham HT, Mesplede T. 2018. The latest evidence for possible HIV-1 curative strategies. Drugs
878 Context 7:212522.
879 3. Collier DA, Monit C, Gupta RK. 2019. The Impact of HIV-1 Drug Escape on the Global
880 Treatment Landscape. Cell Host Microbe 26:48-60.
881 4. Boender TS, Sigaloff KC, McMahon JH, Kiertiburanakul S, Jordan MR, Barcarolo J, Ford N,
882 Rinke de Wit TF, Bertagnolio S. 2015. Long-term Virological Outcomes of First-Line
883 Antiretroviral Therapy for HIV-1 in Low- and Middle-Income Countries: A Systematic Review
884 and Meta-analysis. Clin Infect Dis 61:1453-61.
885 5. Gregson J, Kaleebu P, Marconi VC, van Vuuren C, Ndembi N, Hamers RL, Kanki P, Hoffmann
886 CJ, Lockman S, Pillay D, de Oliveira T, Clumeck N, Hunt G, Kerschberger B, Shafer RW, Yang
887 C, Raizes E, Kantor R, Gupta RK. 2017. Occult HIV-1 drug resistance to thymidine analogues
888 following failure of first-line tenofovir combined with a cytosine analogue and nevirapine or
889 efavirenz in sub Saharan Africa: a retrospective multi-centre cohort study. Lancet Infect Dis
890 17:296-304.
891 6. Cambiano V, Bertagnolio S, Jordan MR, Pillay D, Perriens JH, Venter F, Lundgren J, Phillips A.
892 2014. Predicted levels of HIV drug resistance: potential impact of expanding diagnosis,
893 retention, and eligibility criteria for antiretroviral therapy initiation. AIDS 28 Suppl 1:S15-23.
894 7. Llibre JM. 2017. Time to get serious with HIV-1 resistance in sub-Saharan Africa. Lancet Infect
895 Dis 17:241-243.
896 8. Dionne B. 2019. Key Principles of Antiretroviral Pharmacology. Infect Dis Clin North Am
897 33:787-805.

898 9. Carnes SK, Sheehan JH, Aiken C. 2018. Inhibitors of the HIV-1 capsid, a target of opportunity.
899 Curr Opin HIV AIDS 13:359-365.
900 10. Thenin-Houssier S, Valente ST. 2016. HIV-1 Capsid Inhibitors as Antiretroviral Agents. Curr
901 HIV Res 14:270-82.
902 11. Balasubramaniam M, Zhou J, Addai A, Martinez P, Pandhare J, Aiken C, Dash C. 2019. PF74
903 Inhibits HIV-1 Integration by Altering the Composition of the Preintegration Complex. J Virol
904 93.
905 12. Blair WS, Pickford C, Irving SL, Brown DG, Anderson M, Bazin R, Cao J, Ciaramella G,
906 Isaacson J, Jackson L, Hunt R, Kjerrstrom A, Nieman JA, Patick AK, Perros M, Scott AD,
907 Whitby K, Wu H, Butler SL. 2010. HIV capsid is a tractable target for small molecule
908 therapeutic intervention. PLoS Pathog 6:e1001220.
909 13. Bhattacharya A, Alam SL, Fricke T, Zadrozny K, Sedzicki J, Taylor AB, Demeler B, Pornillos
910 O, Ganser-Pornillos BK, Diaz-Griffero F, Ivanov DN, Yeager M. 2014. Structural basis of HIV-
911 1 capsid recognition by PF74 and CPSF6. Proc Natl Acad Sci U S A 111:18625-30.
912 14. Rankovic S, Ramalho R, Aiken C, Rousso I. 2018. PF74 Reinforces the HIV-1 Capsid To Impair
913 Reverse Transcription-Induced Uncoating. J Virol 92.
914 15. Shi J, Zhou J, Shah VB, Aiken C, Whitby K. 2011. Small-molecule inhibition of human
915 immunodeficiency virus type 1 infection by virus capsid destabilization. J Virol 85:542-9.
916 16. Zhou J, Price AJ, Halambage UD, James LC, Aiken C. 2015. HIV-1 Resistance to the Capsid-
917 Targeting Inhibitor PF74 Results in Altered Dependence on Host Factors Required for Virus
918 Nuclear Entry. J Virol 89:9068-79.
919 17. Yant SR, Mulato A, Hansen D, Tse WC, Niedziela-Majka A, Zhang JR, Stepan GJ, Jin D, Wong
920 MH, Perreira JM, Singer E, Papalia GA, Hu EY, Zheng J, Lu B, Schroeder SD, Chou K,
921 Ahmadyar S, Liclican A, Yu H, Novikov N, Paoli E, Gonik D, Ram RR, Hung M, McDougall
922 WM, Brass AL, Sundquist WI, Cihlar T, Link JO. 2019. A highly potent long-acting small-

923 molecule HIV-1 capsid inhibitor with efficacy in a humanized mouse model. Nat Med 25:1377-
924 1384.
925 18. Fujioka T, Kashiwada Y, Kilkuskie RE, Cosentino LM, Ballas LM, Jiang JB, Janzen WP, Chen
926 IS, Lee KH. 1994. Anti-AIDS agents, 11. Betulinic acid and platanic acid as anti-HIV principles
927 from Syzigium claviflorum, and the anti-HIV activity of structurally related triterpenoids. J Nat
928 Prod 57:243-7.
929 19. Lampel A, Bram Y, Ezer A, Shaltiel-Kario R, Saad JS, Bacharach E, Gazit E. 2015. Targeting
930 the Early Step of Building Block Organization in Viral Capsid Assembly. ACS Chem Biol
931 10:1785-90.
932 20. Machara A, Lux V, Kozisek M, Grantz Saskova K, Stepanek O, Kotora M, Parkan K, Pavova M,
933 Glass B, Sehr P, Lewis J, Muller B, Krausslich HG, Konvalinka J. 2016. Specific Inhibitors of
934 HIV Capsid Assembly Binding to the C-Terminal Domain of the Capsid Protein: Evaluation of
935 2-Arylquinazolines as Potential Antiviral Compounds. J Med Chem 59:545-58.
936 21. Sticht J, Humbert M, Findlow S, Bodem J, Muller B, Dietrich U, Werner J, Krausslich HG.
937 2005. A peptide inhibitor of HIV-1 assembly in vitro. Nat Struct Mol Biol 12:671-7.
938 22. Thenin-Houssier S, de Vera IM, Pedro-Rosa L, Brady A, Richard A, Konnick B, Opp S, Buffone
939 C, Fuhrmann J, Kota S, Billack B, Pietka-Ottlik M, Tellinghuisen T, Choe H, Spicer T,
940 Scampavia L, Diaz-Griffero F, Kojetin DJ, Valente ST. 2016. Ebselen, a Small-Molecule Capsid
941 Inhibitor of HIV-1 Replication. Antimicrob Agents Chemother 60:2195-208.
942 23. Bush DL, Vogt VM. 2014. In Vitro Assembly of Retroviruses. Annu Rev Virol 1:561-80.
943 24. Barajas BC, Tanaka M, Robinson BA, Phuong DJ, Chutiraka K, Reed JC, Lingappa JR. 2018.
944 Identifying the assembly intermediate in which Gag first associates with unspliced HIV-1 RNA
945 suggests a novel model for HIV-1 RNA packaging. PLoS Pathog 14:e1006977.
946 25. Dooher JE, Lingappa JR. 2004. Conservation of a step-wise, energy-sensitive pathway involving
947 HP68 for assembly of primate lentiviral capsids in cells. J Virol 78:1645-56.

948 26. Dooher JE, Schneider BL, Reed JC, Lingappa JR. 2007. Host ABCE1 is at Plasma Membrane
949 HIV Assembly Sites and Its Dissociation from Gag is Linked to Subsequent Events of Virus
950 Production. Traffic 8:195-211.
951 27. Klein KC, Reed JC, Tanaka M, Nguyen VT, Giri S, Lingappa JR. 2011. HIV Gag-leucine zipper
952 chimeras form ABCE1-containing intermediates and RNase-resistant immature capsids similar
953 to those formed by wild-type HIV-1 Gag. J Virol 85:7419-35.
954 28. Lingappa JR, Hill RL, Wong ML, Hegde RS. 1997. A multistep, ATP-dependent pathway for
955 assembly of human immunodeficiency virus capsids in a cell-free system. J Cell Biol 136:567-
956 81.
957 29. Lingappa JR, Newman MA, Klein KC, Dooher JE. 2005. Comparing capsid assembly of primate
958 lentiviruses and hepatitis B virus using cell-free systems. Virology 333:114-23.
959 30. Reed JC, Molter B, Geary CD, McNevin J, McElrath J, Giri S, Klein KC, Lingappa JR. 2012.
960 HIV-1 Gag co-opts a cellular complex containing DDX6, a helicase that facilitates capsid
961 assembly. J Cell Biol 198:439-56.
962 31. Reed JC, Westergreen N, Barajas BC, Ressler DTB, Phuong DJ, Swain JV, Lingappa VR,
963 Lingappa JR. 2018. The formation of RNA granule-derived capsid assembly intermediates
964 appears to be conserved between HIV-1 and the non-primate lentivirus FIV. J Virol
965 doi:10.1128/JVI.01761-17.
966 32. Robinson BA, Reed JC, Geary CD, Swain JV, Lingappa JR. 2014. A temporospatial map that
967 defines specific steps at which critical surfaces in the Gag MA and CA domains act during
968 immature HIV-1 capsid assembly in cells. J Virol 88:5718-41.
969 33. Tanaka M, Robinson BA, Chutiraka K, Geary CD, Reed JC, Lingappa JR. 2015. Mutations of
970 Conserved Residues in the Major Homology Region Arrest Assembling HIV-1 Gag as a
971 Membrane-Targeted Intermediate Containing Genomic RNA and Cellular Proteins. J Virol
972 90:1944-63.

973 34. Zimmerman C, Klein KC, Kiser PK, Singh ARS, Firestein BL, Riba SC, Lingappa JR. 2002.
974 Identification of a host protein essential for assembly of immature HIV-1 capsids. Nature
975 415:88-92.
976 35. Lingappa UF, Wu X, Macieik A, Yu SF, Atuegbu A, Corpuz M, Francis J, Nichols C, Calayag
977 A, Shi H, Ellison JA, Harrell EK, Asundi V, Lingappa JR, Prasad MD, Lipkin WI, Dey D, Hurt
978 CR, Lingappa VR, Hansen WJ, Rupprecht CE. 2013. Host-rabies virus protein-protein
979 interactions as druggable antiviral targets. Proceedings of the National Academy of Sciences of
980 the United States of America 110:E861-8.
981 36. Freienstein C, Blobel G. 1974. Use of eukaryotic native small ribosomal subunits for the
982 translation of globin messenger RNA. Proc Natl Acad Sci U S A 71:3435-9.
983 37. Singh AR, Hill RL, Lingappa JR. 2001. Effect of mutations in Gag on assembly of immature
984 human immunodeficiency virus type 1 capsids in a cell-free system. Virology 279:257-70.
985 38. Lingappa JR, Dooher JE, Newman MA, Kiser PK, Klein KC. 2006. Basic residues in the
986 nucleocapsid domain of Gag are required for interaction of HIV-1 gag with ABCE1 (HP68), a
987 cellular protein important for HIV-1 capsid assembly. J Biol Chem 281:3773-84.
988 39. Tritel M, Resh MD. 2001. The late stage of human immunodeficiency virus type 1 assembly is
989 an energy-dependent process. J Virol 75:5473-81.
990 40. Soderberg O, Gullberg M, Jarvius M, Ridderstrale K, Leuchowius KJ, Jarvius J, Wester K,
991 Hydbring P, Bahram F, Larsson LG, Landegren U. 2006. Direct observation of individual
992 endogenous protein complexes in situ by proximity ligation. Nat Methods 3:995-1000.
993 41. Shafer RW, Schapiro JM. 2005. Drug resistance and antiretroviral drug development. J
994 Antimicrob Chemother 55:817-20.
995 42. Gupta A, Jamal S, Goyal S, Jain R, Wahi D, Grover A. 2015. Structural studies on molecular
996 mechanisms of Nelfinavir resistance caused by non-active site mutation V77I in HIV-1 protease.
997 BMC Bioinformatics 16 Suppl 19:S10.

998 43. Perry CM, Frampton JE, McCormack PL, Siddiqui MA, Cvetkovic RS. 2005. Nelfinavir: a
999 review of its use in the management of HIV infection. Drugs 65:2209-44.
1000 44. Rhee SY, Gonzales MJ, Kantor R, Betts BJ, Ravela J, Shafer RW. 2003. Human
1001 immunodeficiency virus reverse transcriptase and protease sequence database. Nucleic Acids
1002 Res 31:298-303.
1003 45. Rhee SY, Taylor J, Wadhera G, Ben-Hur A, Brutlag DL, Shafer RW. 2006. Genotypic predictors
1004 of human immunodeficiency virus type 1 drug resistance. Proc Natl Acad Sci U S A 103:17355-
1005 60.
1006 46. Weber IT, Agniswamy J. 2009. HIV-1 Protease: Structural Perspectives on Drug Resistance.
1007 Viruses 1:1110-36.
1008 47. Gatanaga H, Das D, Suzuki Y, Yeh DD, Hussain KA, Ghosh AK, Mitsuya H. 2006. Altered
1009 HIV-1 Gag protein interactions with cyclophilin A (CypA) on the acquisition of H219Q and
1010 H219P substitutions in the CypA binding loop. J Biol Chem 281:1241-50.
1011 48. Kuiken C, Foley B, Hahn B, Marx P, McCutchan F, Mellors JW, Mullins J, Wolinsky S, Korber
1012 B. 2000. Human Retroviruses and AIDS Los Alamaos National Laboratory, Los Alamos, NM.
1013 49. Dicker I, Zhang S, Ray N, Beno BR, Regueiro-Ren A, Joshi S, Cockett M, Krystal M, Lataillade
1014 M. 2019. Resistance profile of the HIV-1 maturation inhibitor GSK3532795 in vitro and in a
1015 clinical study. PLoS One 14:e0224076.
1016 50. Gatanaga H, Suzuki Y, Tsang H, Yoshimura K, Kavlick MF, Nagashima K, Gorelick RJ, Mardy
1017 S, Tang C, Summers MF, Mitsuya H. 2002. Amino acid substitutions in Gag protein at non-
1018 cleavage sites are indispensable for the development of a high multitude of HIV-1 resistance
1019 against protease inhibitors. J Biol Chem 277:5952-61.
1020 51. Van Duyne R, Kuo LS, Pham P, Fujii K, Freed EO. 2019. Mutations in the HIV-1 envelope
1021 glycoprotein can broadly rescue blocks at multiple steps in the virus replication cycle. Proc Natl
1022 Acad Sci U S A 116:9040-9049.

1023 52. Hermann FG, Egerer L, Brauer F, Gerum C, Schwalbe H, Dietrich U, von Laer D. 2009.
1024 Mutations in gp120 contribute to the resistance of human immunodeficiency virus type 1 to
1025 membrane-anchored C-peptide maC46. J Virol 83:4844-53.
1026 53. Kinomoto M, Yokoyama M, Sato H, Kojima A, Kurata T, Ikuta K, Sata T, Tokunaga K. 2005.
1027 Amino acid 36 in the human immunodeficiency virus type 1 gp41 ectodomain controls fusogenic
1028 activity: implications for the molecular mechanism of viral escape from a fusion inhibitor. J
1029 Virol 79:5996-6004.
1030 54. Nameki D, Kodama E, Ikeuchi M, Mabuchi N, Otaka A, Tamamura H, Ohno M, Fujii N,
1031 Matsuoka M. 2005. Mutations conferring resistance to human immunodeficiency virus type 1
1032 fusion inhibitors are restricted by gp41 and Rev-responsive element functions. J Virol 79:764-70.
1033 55. Garbelli A, Riva V, Crespan E, Maga G. 2017. How to win the HIV-1 drug resistance hurdle
1034 race: running faster or jumping higher? Biochem J 474:1559-1577.
1035 56. Ji X, Li Z. 2020. Medicinal chemistry strategies toward host targeting antiviral agents. Med Res
1036 Rev doi:10.1002/med.21664.
1037 57. Lemke CT, Titolo S, von Schwedler U, Goudreau N, Mercier JF, Wardrop E, Faucher AM,
1038 Coulombe R, Banik SS, Fader L, Gagnon A, Kawai SH, Rancourt J, Tremblay M, Yoakim C,
1039 Simoneau B, Archambault J, Sundquist WI, Mason SW. 2012. Distinct effects of two HIV-1
1040 capsid assembly inhibitor families that bind the same site within the N-terminal domain of the
1041 viral CA protein. J Virol 86:6643-55.
1042 58. Li F, Goila-Gaur R, Salzwedel K, Kilgore NR, Reddick M, Matallana C, Castillo A, Zoumplis D,
1043 Martin DE, Orenstein JM, Allaway GP, Freed EO, Wild CT. 2003. PA-457: a potent HIV
1044 inhibitor that disrupts core condensation by targeting a late step in Gag processing. Proc Natl
1045 Acad Sci U S A 100:13555-60.

1046 59. Vozzolo L, Loh B, Gane PJ, Tribak M, Zhou L, Anderson I, Nyakatura E, Jenner RG, Selwood
1047 D, Fassati A. 2010. Gyrase B inhibitor impairs HIV-1 replication by targeting Hsp90 and the
1048 capsid protein. J Biol Chem 285:39314-28.
1049 60. Beliakova-Bethell N, Beckham C, Giddings TH, Jr., Winey M, Parker R, Sandmeyer S. 2006.
1050 Virus-like particles of the Ty3 retrotransposon assemble in association with P-body components.
1051 RNA 12:94-101.
1052 61. Bilanchone V, Clemens K, Kaake R, Dawson AR, Matheos D, Nagashima K, Sitlani P, Patterson
1053 K, Chang I, Huang L, Sandmeyer S. 2015. Ty3 Retrotransposon Hijacks Mating Yeast RNA
1054 Processing Bodies to Infect New Genomes. PLoS Genet 11:e1005528.
1055 62. Irwin B, Aye M, Baldi P, Beliakova-Bethell N, Cheng H, Dou Y, Liou W, Sandmeyer S. 2005.
1056 Retroviruses and yeast retrotransposons use overlapping sets of host genes. Genome Res 15:641-
1057 54.
1058 63. Yu S, Lujan P, Jackson D, Emerman M, Linial M. 2011. The DEAD-box RNA helicase DDX6 is
1059 required for efficient encapsidation of a retroviral genome. PloS Pathog 7:e1002303.
1060 64. Abrahamyan LG, Chatel-Chaix L, Ajamian L, Milev MP, Monette A, Clement JF, Song R,
1061 Lehmann M, DesGroseillers L, Laughrea M, Boccaccio G, Mouland AJ. 2010. Novel Staufen1
1062 ribonucleoproteins prevent formation of stress granules but favour encapsidation of HIV-1
1063 genomic RNA. J Cell Sci 123:369-83.
1064 65. Chatel-Chaix L, Abrahamyan L, Frechina C, Mouland AJ, DesGroseillers L. 2007. The host
1065 protein Staufen1 participates in human immunodeficiency virus type 1 assembly in live cells by
1066 influencing pr55Gag multimerization. J Virol 81:6216-30.
1067 66. Chatel-Chaix L, Boulay K, Mouland AJ, Desgroseillers L. 2008. The host protein Staufen1
1068 interacts with the Pr55Gag zinc fingers and regulates HIV-1 assembly via its N-terminus.
1069 Retrovirology 5:41.

1070 67. Rao S, Hassine S, Monette A, Amorim R, DesGroseillers L, Mouland AJ. 2019. HIV-1 requires
1071 Staufen1 to dissociate stress granules and to produce infectious viral particles. RNA 25:727-736.
1072 68. Burdick R, Smith JL, Chaipan C, Friew Y, Chen J, Venkatachari NJ, Delviks-Frankenberry KA,
1073 Hu WS, Pathak VK. 2010. P body-associated protein Mov10 inhibits HIV-1 replication at
1074 multiple stages. J Virol 84:10241-53.
1075 69. Furtak V, Mulky A, Rawlings SA, Kozhaya L, Lee K, Kewalramani VN, Unutmaz D. 2010.
1076 Perturbation of the P-body component Mov10 inhibits HIV-1 infectivity. PloS one 5:e9081.
1077 70. Adachi A, Gendelman HE, Koenig S, Folks T, Willey R, Rabson A, Martin MA. 1986.
1078 Production of acquired immunodeficiency syndrome-associated retrovirus in human and
1079 nonhuman cells transfected with an infectious molecular clone. J Virol 59:284-91.
1080 71. Rogel ME, Wu LI, Emerman M. 1995. The human immunodeficiency virus type 1 vpr gene
1081 prevents cell proliferation during chronic infection. J Virol 69:882-8.
1082 72. Gibson DG, Young L, Chuang RY, Venter JC, Hutchison CA, 3rd, Smith HO. 2009. Enzymatic
1083 assembly of DNA molecules up to several hundred kilobases. Nat Methods 6:343-5.
1084 73. Poss M, Overbaugh J. 1999. Variants from the diverse virus population identified at
1085 seroconversion of a clade A human immunodeficiency virus type 1-infected woman have distinct
1086 biological properties. J Virol 73:5255-64.
1087 74. Provine NM, Puryear WB, Wu X, Overbaugh J, Haigwood NL. 2009. The infectious molecular
1088 clone and pseudotyped virus models of human immunodeficiency virus type 1 exhibit significant
1089 differences in virion composition with only moderate differences in infectivity and inhibition
1090 sensitivity. J Virol 83:9002-7.
1091 75. Wu X, Parast AB, Richardson BA, Nduati R, John-Stewart G, Mbori-Ngacha D, Rainwater SM,
1092 Overbaugh J. 2006. Neutralization escape variants of human immunodeficiency virus type 1 are
1093 transmitted from mother to infant. J Virol 80:835-44.

1094 76. Neumann G, Watanabe T, Ito H, Watanabe S, Goto H, Gao P, Hughes M, Perez DR, Donis R,
1095 Hoffmann E, Hobom G, Kawaoka Y. 1999. Generation of influenza A viruses entirely from
1096 cloned cDNAs. Proc Natl Acad Sci U S A 96:9345-50.
1097 77. Haertle T, Carrera CJ, Wasson DB, Sowers LC, Richman DD, Carson DA. 1988. Metabolism
1098 and anti-human immunodeficiency virus-1 activity of 2-halo-2',3'-dideoxyadenosine derivatives.
1099 J Biol Chem 263:5870-5.
1100 78. Harada S, Koyanagi Y, Yamamoto N. 1985. Infection of HTLV-III/LAV in HTLV-I-carrying
1101 cells MT-2 and MT-4 and application in a plaque assay. Science 229:563-6.
1102 79. Boyd DF, Peterson D, Haggarty BS, Jordan AP, Hogan MJ, Goo L, Hoxie JA, Overbaugh J.
1103 2015. Mutations in HIV-1 envelope that enhance entry with the macaque CD4 receptor alter
1104 antibody recognition by disrupting quaternary interactions within the trimer. J Virol 89:894-907.
1105 80. Derdeyn CA, Decker JM, Sfakianos JN, Wu X, O'Brien WA, Ratner L, Kappes JC, Shaw GM,
1106 Hunter E. 2000. Sensitivity of human immunodeficiency virus type 1 to the fusion inhibitor T-20
1107 is modulated by coreceptor specificity defined by the V3 loop of gp120. J Virol 74:8358-67.
1108 81. Platt EJ, Bilska M, Kozak SL, Kabat D, Montefiori DC. 2009. Evidence that ecotropic murine
1109 leukemia virus contamination in TZM-bl cells does not affect the outcome of neutralizing
1110 antibody assays with human immunodeficiency virus type 1. J Virol 83:8289-92.
1111 82. Platt EJ, Wehrly K, Kuhmann SE, Chesebro B, Kabat D. 1998. Effects of CCR5 and CD4 cell
1112 surface concentrations on infections by macrophagetropic isolates of human immunodeficiency
1113 virus type 1. J Virol 72:2855-64.
1114 83. Takeuchi Y, McClure MO, Pizzato M. 2008. Identification of gammaretroviruses constitutively
1115 released from cell lines used for human immunodeficiency virus research. J Virol 82:12585-8.
1116 84. Wei X, Decker JM, Liu H, Zhang Z, Arani RB, Kilby JM, Saag MS, Wu X, Shaw GM, Kappes
1117 JC. 2002. Emergence of resistant human immunodeficiency virus type 1 in patients receiving
1118 fusion inhibitor (T-20) monotherapy. Antimicrob Agents Chemother 46:1896-905.

1119 85. Chesebro B, Wehrly K, Nishio J, Perryman S. 1992. Macrophage-tropic human
1120 immunodeficiency virus isolates from different patients exhibit unusual V3 envelope sequence
1121 homogeneity in comparison with T-cell-tropic isolates: definition of critical amino acids
1122 involved in cell tropism. J Virol 66:6547-54.
1123 86. Lutz A, Dyall J, Olivo PD, Pekosz A. 2005. Virus-inducible reporter genes as a tool for detecting
1124 and quantifying influenza A virus replication. J Virol Methods 126:13-20.
1125 87. Vermeire J, Naessens E, Vanderstraeten H, Landi A, Iannucci V, Van Nuffel A, Taghon T,
1126 Pizzato M, Verhasselt B. 2012. Quantification of reverse transcriptase activity by real-time PCR
1127 as a fast and accurate method for titration of HIV, lenti- and retroviral vectors. PLoS One
1128 7:e50859.
1129 88. Reed LJ, Muench H. 1938. A simple method of estimating fifty percent endpoints. Am J Hyg
1130 27:493-497.
1131 89. Schindelin J, Arganda-Carreras I, Frise E, Kaynig V, Longair M, Pietzsch T, Preibisch S,
1132 Rueden C, Saalfeld S, Schmid B, Tinevez JY, White DJ, Hartenstein V, Eliceiri K, Tomancak P,
1133 Cardona A. 2012. Fiji: an open-source platform for biological-image analysis. Nat Methods
1134 9:676-82.
1135
1136
1137
1138
1139
1140
1141
1142
1143

1144 **FIGURE LEGENDS**

1145 **FIG 1. The HIV-1 life cycle, assembly pathway, and assembly plate screen.** (A) Schematic
1146 showing the HIV-1 lifecycle, with expression of the integrated provirus, followed by the late and early
1147 phases of the lifecycle, ending with integration in a newly infected cell. The different stages of the virus
1148 lifecycle are indicated in blue. Examples of ARV drugs currently in use are in red, with black labels
1149 under blockade arrows indicating the targets of these drugs. Pink line indicates late events in the viral
1150 lifecycle that are not targeted by currently approved ARV drugs. (B) Schematic showing the host-
1151 catalyzed HIV-1 assembly pathway, starting with Gag synthesis and formation of the early ~10S
1152 assembly intermediate. Next, the cytosolic ~80S intermediate forms when ~10S Gag co-opts a host
1153 RNP complex that contains ABCE1 and the RNA granule protein DDX6, two host enzymes that have
1154 been shown to facilitate assembly. The ~80S assembly intermediate appears to target to the plasma
1155 membrane where Gag multimerization continues resulting in formation of the ~150S and subsequently
1156 the ~500S late assembly intermediate. When assembly of ~750S immature capsid is completed, the host
1157 RNP complex is released. References are in the text. (C) Schematic showing the cell-free protein
1158 synthesis and assembly plate screen that was utilized to identify small molecule inhibitors of the host-
1159 catalyzed pathway of HIV-1 assembly. Briefly, anti-Gag antibody (capture antibody) binds Gag
1160 monomers, oligomers, and multimers generated in a cell-free assembly reaction. The same Gag
1161 antibody is used as a detection antibody that binds to captured oligomers and multimers, but not
1162 monomers, in proportion to the amount of multimerization, thereby generating a larger fluorescent
1163 signal when multimerization occurs. The upper diagram shows anti-Gag antibodies capturing and
1164 detecting Gag oligomers and multimers in assembly intermediates formed during an HIV-1 cell-free
1165 assembly reaction carried out in the presence of DMSO, which does not inhibit assembly. The lower
1166 diagram shows that adding an assembly inhibitor at the start of the cell-free reaction causes fewer Gag
1167 oligomers and multimers to be produced, thereby reducing the detection antibody signal relative to
1168 signal in the DMSO control.

1169 **FIG. 2. PAV-117, identified using cell-extract-based assembly screens, inhibits replication of HIV-**
1170 **1, but not FIV or FLUV, in cell culture.** (A) Schematic showing the cell-free assembly screening
1171 strategy used to identify PAV-117. Small molecules from a library of 150,000 compounds were assayed
1172 in cell-free screens that recapitulate assembly of eight different viral capsids, with each screen being
1173 analogous to the HIV-1 screen in (Fig 1C). Results from the library screens led to generation of a
1174 master hit collection of 249 small molecules that displayed inhibitory activity in one or more of the eight
1175 cell-free assembly screens. Compounds in the master hit collection were assayed for inhibition of HIV-
1176 1 replication in MT-2 T cells, with PAV-117 identified as the compound with optimal EC50, CC50, and
1177 other characteristics in the MT-2 assay. (B) The chemical structure of PAV-117, a
1178 tetrahydroisoquinolone. (C) To determine the EC50 of PAV-117 against HIV-1 replication, a dose-
1179 response curve for inhibition of HIV-1 replication by PAV-117 was generated by treating human MT-2
1180 T cells with indicated doses of PAV-117 followed by infection with a replication-competent HIV-1
1181 NL4-3 RLuc reporter virus (MOI of 0.02). After 96 h of spreading infection, luciferase activity was
1182 measured as an indicator of HIV-1 replication and is displayed as inhibition of replication relative to
1183 DMSO-treated controls (% inhibition). CC50 was determined in parallel using uninfected MT-2 T cells
1184 and is marked by a vertical dashed line. Error bars show standard error of the mean (SEM) determined
1185 from three replicates. (D) The graph shows quantification of infectious FLUV in MDCK cells treated
1186 with DMSO or with either PAV-117 or Tamiflu at a concentration 20-fold higher than the EC50 for
1187 each drug (0.8 μM for PAV-117, 10 μM for Tamiflu). Treated cells were infected with FLUV (strain
1188 WSN/33(H1N1), MOI of 0.001) and viral titer was measured after 24 h by TCID50. (E) To determine
1189 the EC50 of PAV-117 against FIV replication, a dose-response curve for inhibition of FIV replication by
1190 PAV-117 was generated by treatment of G355-5 cells with indicated doses of PAV-117 followed by
1191 infection with FIV 34TF10 (1954 nU of RT activity per well). After 144 h of spreading infection, RT
1192 activity was measured and used to calculate inhibition of FIV replication relative to DMSO controls (%
1193 inhibition). CC50 was determined in parallel using uninfected G355-5 cells and is marked by a vertical

1194 dashed line. Error bars show SEM determined from three replicates. (E) Quantification of replication of
1195 an HIV-1 primary isolate. SupT1.CCR5 cells were treated with 0.37 μM PAV-117 or DMSO followed
1196 by infection with HIV-1 Q23.BG505, a CCR5-tropic subtype A molecular clone. HIV-1 replication
1197 proceeded for 96 h followed by measurement of HIV-1 infectivity in the culture supernatant using the
1198 MUG assay in TZM-bl cells.
1199
1200 **FIG. 3. PAV-117 acts late in the HIV-1 life cycle, inhibiting virus production but not specific**
1201 **infectivity.** (A) Schematic of the early assay, which measures effects on viral entry through early viral
1202 gene expression. MT-2 cells were infected with the single-round HIV-1 pNL4-3 RLuc virus (*env*-
1203 deleted and pseudotyped with HIV-1 NL4-3 Env) in the presence of compound or DMSO. After 48 h,
1204 luciferase activity was measured and used to calculate inhibition of HIV-1 replication relative to the
1205 DMSO control (% inhibition). The graph shows the dose-response curve for inhibition of HIV-1 early
1206 events by PAV-117 that was generated using this assay and used to determine the EC50. CC50 was
1207 determined in parallel using uninfected MT-2 T cells and is marked by a vertical dashed line. Error bars
1208 in graph show SEM determined from three replicates. (B) Schematic of the late assays, which measure
1209 effects on viral late events starting with expression of Gag and GagPol through virus release and
1210 maturation. Chronically infected H9 T cells (H9-HIV) were treated with either compound or DMSO,
1211 and media collected 48 h later were used for two assays: 1) to quantify inhibition of HIV-1 infectivity
1212 relative to DMSO control by titering on TZM-bl cells (black curve, used to calculate EC50 for inhibition
1213 of infectivity) and 2) to quantify inhibition of virus production by pelleting virus for western blot (WB)
1214 with antibody to HIV-1 Gag (αGag; blue curve, used to calculate EC50 for inhibition of virus
1215 production). The CC50 was determined in the inhibition assay and is marked by a vertical dashed line.
1216 A representative αGag WB of virus pellets is shown below the dose-response graph, with DMSO
1217 treatment or concentration of PAV-117 indicated above each WB lane and % inhibition of virus

1218 production (relative to the DMSO-treated control) indicated below each lane. Error bars in (B) and (C)
1219 show SEM determined from two replicates.
1220
1221 **FIG. 4. PAV-117 appears to act during the HIV-1 assembly pathway, after formation of the ~80S**
1222 **intermediate.** MT-2 cells were infected with HIV-1 LAI *pro*- Δ*env* (pseudotyped with HIV-1 NL4-3
1223 Env) and treated with DMSO or the indicated concentrations of PAV-117 for 48 h. (A) Media and cell
1224 lysates were harvested to analyze effects on virus production and intracellular steady-state Gag levels, as
1225 indicated, using WB with Gag antibody (αGag) to quantify p24 or p55 Gag. (B) Cell lysates were also
1226 analyzed for intracellular steady-state levels of two cellular proteins, GAPDH and actin, by WB with
1227 αGAPDH and αactin. For (A) and (B), data in graphs are shown as % of DMSO-treated controls, with
1228 error bars showing SEM from two replicates, and representative WBs are shown below graphs, (C) To
1229 quantify intracellular steady-state levels of assembly intermediates, cell lysates from panels A and B
1230 were also analyzed by velocity sedimentation followed by WB of each gradient fraction with αGag.
1231 Fraction numbers are indicated above the WB panels, with migration of specific assembly intermediates
1232 indicated by brackets above. Graphs show quantification of p55 Gag in fractions containing the ~10S,
1233 ~80S/150S, and ~500S intermediates as percent of total p55 Gag in the gradient. Expected migration of
1234 each protein in WB panels is indicated to the right.
1235
1236 **FIG. 5. Analysis of structure-activity relationships identified an analog that potently inhibits**
1237 **HIV-1 replication in PBMCs and a site for tags.** (A) The general chemical structure of PAV-117
1238 analogs is shown at left indicating the R1, R2, and R3 positions in the pendant benzene ring. The table
1239 shows results obtained for analogs in which the R1, R2, and R3 positions contain hydrogen, methyl,
1240 methoxy, or benzoyloxy groups as indicated, including the EC50 for inhibition of HIV-1 replication in
1241 MT-2 cells and the CC50 in MT-2 cells (assays described in Fig. 2C). Values are shown as the average
1242 of multiple independent repeats ×/÷ GSD, with *n* = the number of independent repeats. Also shown is

1243 the selectivity index (SI), which is equivalent to CC50/EC50. (B) The structure of PAV-206 is shown at
1244 left. The blue dose-response curve shows inhibition of HIV-1 replication by PAV-206 in MT-2 T cells
1245 (using the assay described in Fig. 2C). The orange dose-response curve shows inhibition of HIV-1
1246 replication by PAV-206 in PHA-activated PBMC infected with unmodified HIV-1 NL4-3 at an MOI of
1247 0.008. (C) Shown on the left is the structure of PAV-818, the biotinylated analog of PAV-206, and on
1248 the right a dose-response curve for inhibition of HIV-1 replication by PAV-818 in MT-2 T cells (assays
1249 as in Fig. 2C). In the PAV-818 structure, the biotin moiety is shown in red. A diazirine group in the
1250 PAV-818 structure is shown in blue; this group was added for future crosslinking studies but is not used
1251 in the current study. For all graphs in (B) and (C), the indicated EC50s were determined from the dose-
1252 response curves; CC50s were determined in uninfected cells in parallel and are marked by vertical
1253 dashed lines. Error bars in (B) and (C) show SEM from three replicates.
1254
1255 **FIG. 6. An antiviral analog of PAV-206 colocalizes with HIV-1 Gag *in situ*.** (A) Schematic of the
1256 PLA approach for detecting colocalization of compound with Gag. 293T cells chronically infected with
1257 HIV-1 (293T-HIV) or uninfected 293T cells were treated with indicated amounts of PAV-818 (the
1258 biotinylated active compound), PAV-543 (the biotinylated inactive compound), or DMSO for 16 h.
1259 PLA was performed by incubating with primary antibodies (rabbit anti-biotin and mouse anti-Gag)
1260 followed by PLA secondary antibodies (anti-rabbit IgG coupled to (+) PLA oligo and anti-mouse IgG
1261 coupled to (-) PLA oligo). Addition of other PLA reagents leads to connector oligos linking the (+) and
1262 (-) oligos only if the primary antibodies are colocalized; this in turn results in the PLA amplification
1263 reaction. Addition of an oligo that recognizes a sequence in the amplified regions and is coupled to a
1264 red fluorophore (red star) results in intense spots at sites where biotinylated compound and Gag are
1265 colocalized *in situ*. Following PLA, indirect immunofluorescence (IF) is performed by adding
1266 secondary antibody conjugated to a green fluorophore (green star) to detect any unoccupied Gag
1267 antibody, thus marking Gag-expressing cells with low-level green fluorescence (B) The graph shows

1268 the average number of biotin-Gag PLA spots per cell for each condition, with + indicating HIV-1-
1269 infected cells and – indicating uninfected cells. Twenty fields were analyzed for each group (containing
1270 a total of 186 - 316 cells per group), with error bars showing SEM. * indicates a significant difference
1271 in the number of biotin-Gag PLA spots per cell when comparing treatment with PAV-818 vs. PAV-543,
1272 both at 10 μM ($p < 0.001$). (C) A representative field for each group quantified in (B) is shown, except
1273 for DMSO treatment. Fields on the left show biotin-Gag PLA spots alone in grayscale. To the right are
1274 the same fields shown as a merge of three color-channels: biotin-Gag PLA (red), Gag IF (green), and
1275 DAPI-stained nuclei (blue). Scale bars, 10 μm.
1276
1277 **FIG. 7. Resistance mutations in *gag* or *pol* were not observed upon selection with PAV-206 in cell**
1278 **culture.** (A) A NL4-3 virus stock was passaged weekly for 37 weeks in the presence of either PAV-206
1279 or nelfinavir starting at a concentration of 1 x EC50. The concentration of compound was increased
1280 two-fold when compound-treated cultures reached maximum viral cytopathic effect (CPE) in a
1281 timeframe similar to a parallel DMSO control. The graph shows the compound concentration as fold-
1282 EC50 vs. week of selection (passage #) for PAV-206 (left) or nelfinavir (right). Red arrows indicate
1283 passages where virus was amplified, either with sequencing of *gag* alone, *gag* & *protease*, or the full
1284 genome minus the LTRs (as indicated above red arrows). (B) For each selection (PAV-206 vs.
1285 nelfinavir), an HIV-1 genome map is shown, with positions of viral open reading frames (ORFs), 5'
1286 LTR, and 3' LTR, with a line below indicating their approximate nucleotide positions within the HIV-1
1287 genome. In each case, ORFs in which dominant non-synonymous mutations emerged during selection
1288 are color-coded as follows: *gag*, blue; *pro*, red; *env*, brown. Beneath the HIV-1 genome maps, dominant
1289 non-synonymous amino acid mutations (identified through sequencing of passages indicated with red
1290 arrows in panel (A)) are shown according to their position in the genome map at the top of panel (B).
1291 The passage (P) in which these mutations were identified is indicated to the left of each genome map
1292 line. The amino acid mutations are color-coded according to the ORF in which they were found (colors

1293 described above). As indicated in boxed legend, which applies to both panels, cyclophilin A binding
1294 loop mutations that have been previously identified as tissue culture adaptations are marked with a
1295 dagger symbol and previously described nelfinavir-specific mutations are marked with an asterisk (with
1296 all references for these in the text and Tables S1 and S2).
1297
1298 **FIG. 8. An antiviral PAV-206 analog colocalizes *in situ* with ABCE1, a host component of**
1299 **assembly intermediates.** (A) Schematic of the PLA approach for detecting colocalization of compound
1300 with ABCE1. 293T cells chronically infected with HIV-1 (293T-HIV) or uninfected 293T cells were
1301 treated with indicated amounts of PAV-818 (the biotinylated active compound), PAV-543 (the
1302 biotinylated inactive compound), or DMSO for 16 h. PLA was performed by incubating with primary
1303 antibodies (mouse anti-biotin and rabbit anti-ABCE1) followed by PLA secondary antibodies (anti-
1304 mouse IgG coupled to (-) PLA oligo and anti-rabbit IgG coupled to (+) PLA oligo). Addition of other
1305 PLA reagents leads to connector oligos linking the (+) and (-) oligos only if the primary antibodies are
1306 colocalized; this in turn results in the PLA amplification reaction. Addition of an oligo that recognizes a
1307 sequence in the amplified regions and is coupled to a red fluorophore (red star) results in intense red
1308 spots at sites where biotinylated compound and ABCE1 are colocalized *in situ*. Following PLA, indirect
1309 immunofluorescence (IF) is performed by adding secondary antibody conjugated to a green fluorophore
1310 (green star) to detect any unoccupied ABCE1 antibody, thus marking intracellular ABCE1 with low-
1311 level green fluorescence (B) The graph shows the average number of biotin-ABCE1 PLA spots per cell
1312 for each condition, with + indicating HIV-1-infected cells and – indicating uninfected cells. Ten fields
1313 were analyzed for each group (containing a total of 104 - 155 cells per group), with error bars showing
1314 SEM. * indicates a significant difference in the number of biotin-ABCE1 PLA spots per cell when
1315 comparing treatment with PAV-818 vs. PAV-543, both at 10 μM ($p < 0.001$). (C) A representative field
1316 for each group quantified in (B) is shown, except for DMSO treatment. Fields on the left show biotin-
1317 ABCE1 PLA spots alone in grayscale. To the right are the same fields shown as a merge of three color-

1318 channels: biotin-ABCE1 PLA (red), ABCE1 IF (green), and DAPI-stained nuclei (blue). Scale bars, 10
1319 μm.
1320
1321 **FIG. 9. An antiviral PAV-206 analog colocalizes *in situ* with DDX6, an RNA granule protein in**
1322 **assembly intermediates that colocalizes with ABCE1.** (A) A schematic of the PLA approach for
1323 detecting colocalization of compound with DDX6 is shown. 293T cells chronically infected with HIV-1
1324 (293T-HIV) were treated with 10 μM PAV-818 (the biotinylated active compound) or DMSO for 16 h.
1325 PLA was performed by incubating with primary antibodies (mouse anti-biotin and rabbit anti-DDX6)
1326 followed by PLA secondary antibodies (anti-mouse IgG coupled to (-) PLA oligo and anti-rabbit IgG
1327 coupled to (+) PLA oligo). Addition of other PLA reagents leads to connector oligos linking the (+) and
1328 (-) oligos only if the primary antibodies are colocalized; this in turn results in the PLA amplification
1329 reaction. Addition of an oligo that recognizes a sequence in the amplified regions and is coupled to a
1330 red fluorophore (red star) results in intense red spots at sites where biotinylated compound and DDX6
1331 are colocalized *in situ*. Following PLA, indirect immunofluorescence (IF) is performed by adding
1332 secondary antibody conjugated to a green fluorophore (green star) to detect any unoccupied DDX6
1333 antibody, thus marking intracellular DDX6 with low-level green fluorescence. The graph shows the
1334 average number of biotin-DDX6 PLA spots per cell for each condition. Five fields were analyzed for
1335 each group (containing a total of 60 - 73 cells per group), with error bars showing SEM. * indicates a
1336 significant difference in the number of biotin-DDX6 PLA spots per cell when comparing treatment with
1337 PAV-818 vs. DMSO ($p < 0.001$). A representative field for each group quantified in the graph is shown,
1338 with images on the left displaying biotin-DDX6 PLA spots alone in grayscale and images on the right
1339 displaying a merge of three color-channels: biotin-DDX6 PLA (red), DDX6 IF (green), and DAPI-
1340 stained nuclei (blue). Scale bars, 10 μm. (B) A schematic of the PLA approach for detecting
1341 colocalization of ABCE1 with DDX6 is shown. 293T cells chronically infected with HIV-1 (293T-
1342 HIV) but not treated with any compounds were analyzed by PLA, as described for (A) above, except the

1343 primary antibodies used were rabbit anti-ABCE1 and mouse anti-DDX6, with red spots representing
1344 sites where ABCE1 and DDX6 are colocalized *in situ*. The graph shows the average number of
1345 ABCE1-DDX6 spots per cell. Ten fields were analyzed (containing a total of 121 cells), with error bars
1346 showing SEM. A representative field is shown, with the image on the left displaying ABCE1-DDX6
1347 PLA spots alone in grayscale and the image on the right displaying a merge of three color-channels:
1348 ABCE1-DDX6 PLA (red), DDX6 IF (green), and DAPI-stained nuclei (blue).
1349
1350 **FIG. 10. A model for the action of PAV-206, a possible first-in-class selective inhibitor of HIV-1**
1351 **assembly.** Upper diagram shows the intracellular pathway for HIV-1 immature capsid assembly, in the
1352 presence of an inactive compound, starting with synthesis of HIV-1 Gag and formation of the early
1353 ~10S assembly intermediate. The ~80S assembly intermediate is formed when HIV-1 Gag co-opts a
1354 host RNP complex related to an RNA granule to form the ~80S cytosolic intermediate. This and
1355 subsequent intermediates contain Gag associated with ABCE1, DDX6, other host factors, and HIV-1
1356 gRNA. After targeting of the cytosolic ~80S assembly intermediate to the host plasma membrane, Gag
1357 multimerization continues leading to the formation of the ~500S assembly intermediate. The host
1358 proteins are released upon formation of the ~750S completed immature capsid, and budding results in
1359 release of the completed immature capsid. The lower diagram shows one model for PAV-117/PAV-206
1360 activity based on the findings in this study. Our colocalization studies suggest that the compound is
1361 associated with both the HIV-1 assembly intermediates and the host RNA-granule-related complex from
1362 which they are derived, since we find the compound colocalized with a host component of this complex,
1363 ABCE1, in the presence and absence of Gag. Additionally, we observed a reduction of virus production
1364 and the amount of ~500S assembly intermediate in PAV-117-treated infected cells. Thus, we
1365 hypothesize that PAV-117/PAV-206 inhibits virus production by acting during the HIV-1 immature
1366 capsid assembly pathway to inhibit progression past the ~80S/150S assembly intermediate.
1367

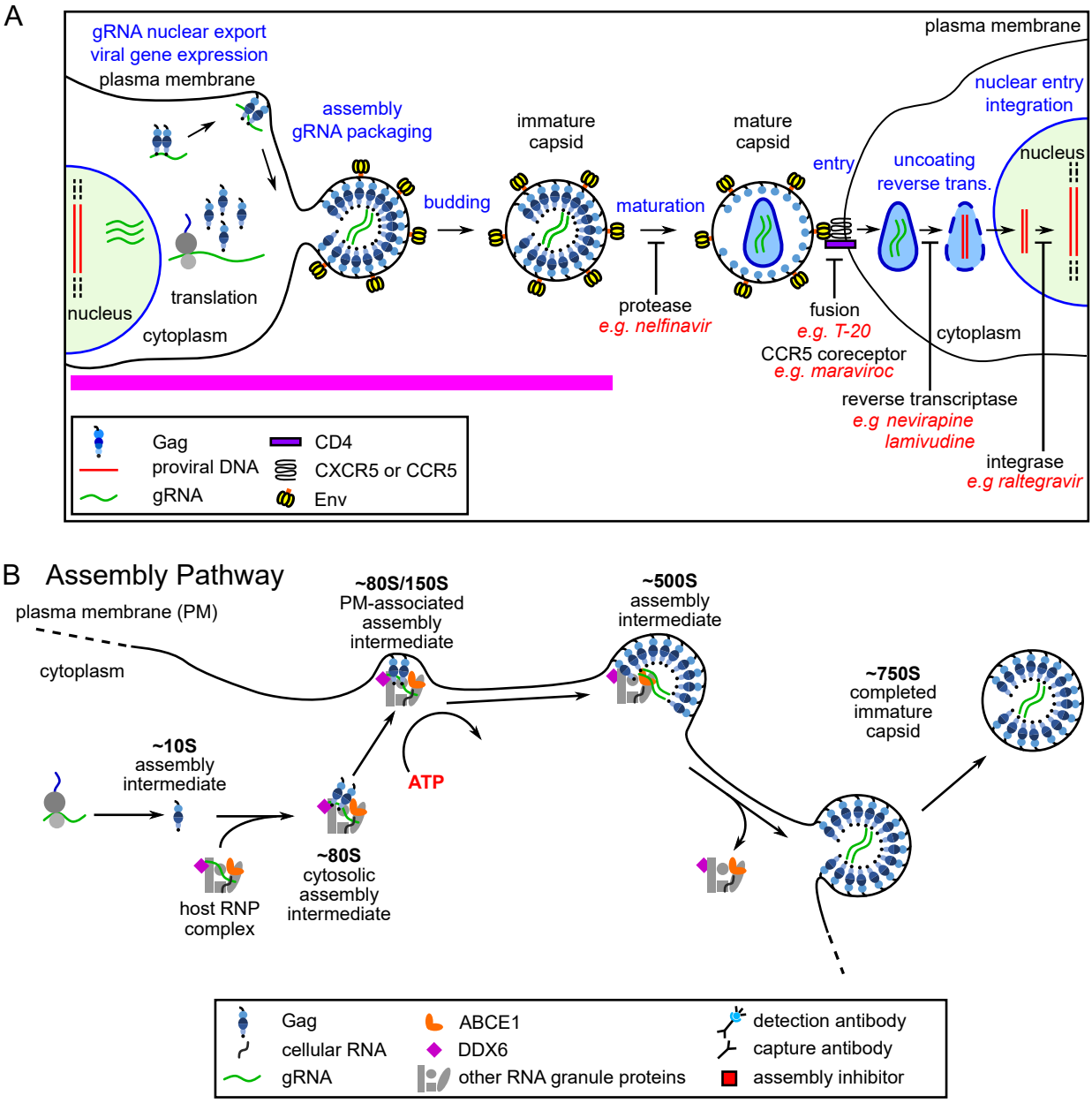

FIG 1 The HIV-1 life cycle, assembly pathway, and assembly plate screen.

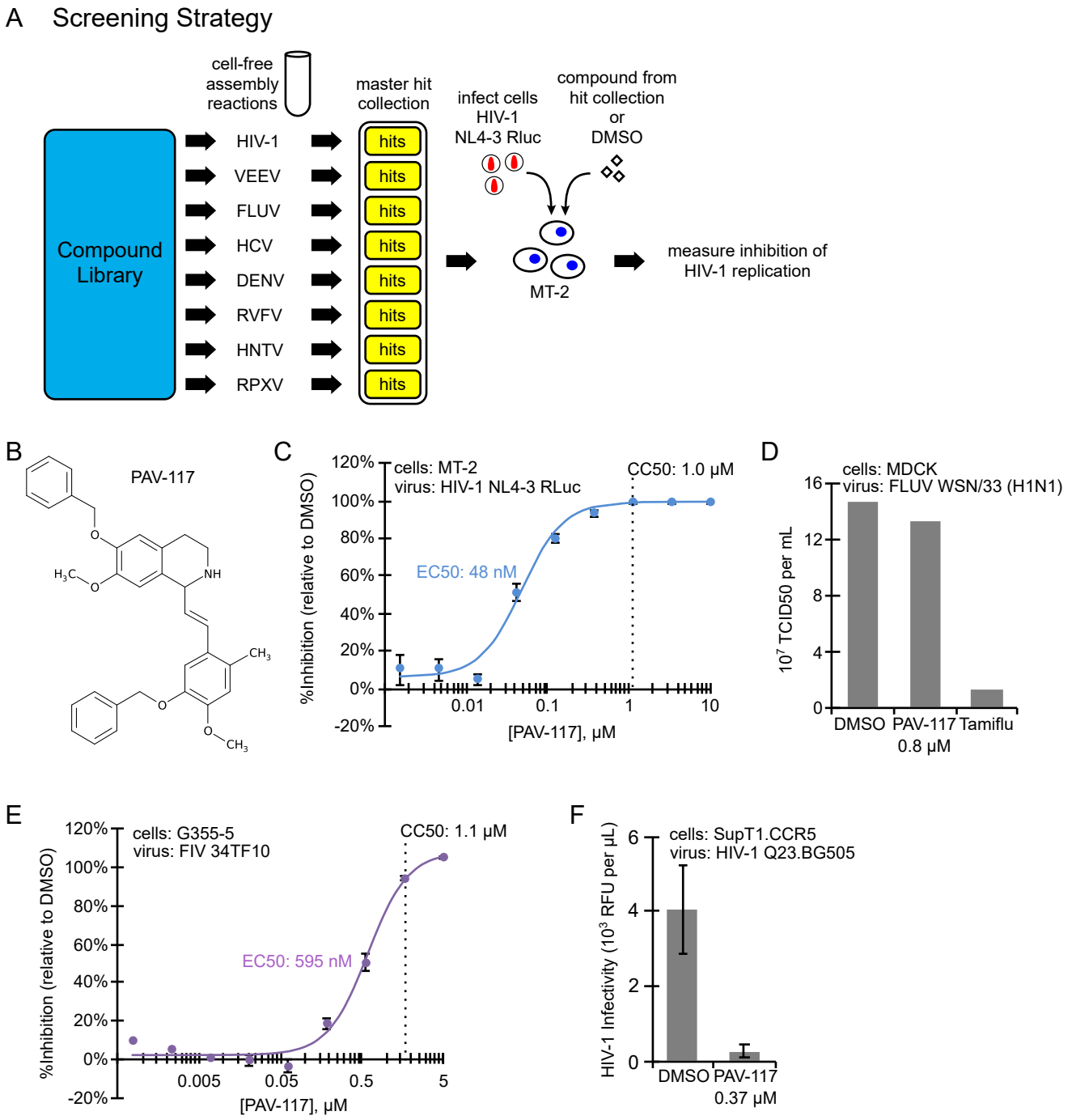

FIG 2 PAV-117, identified using cell-extract-based assembly screens, inhibits replication of HIV-1, but not FLUV and FIV, in cell culture.

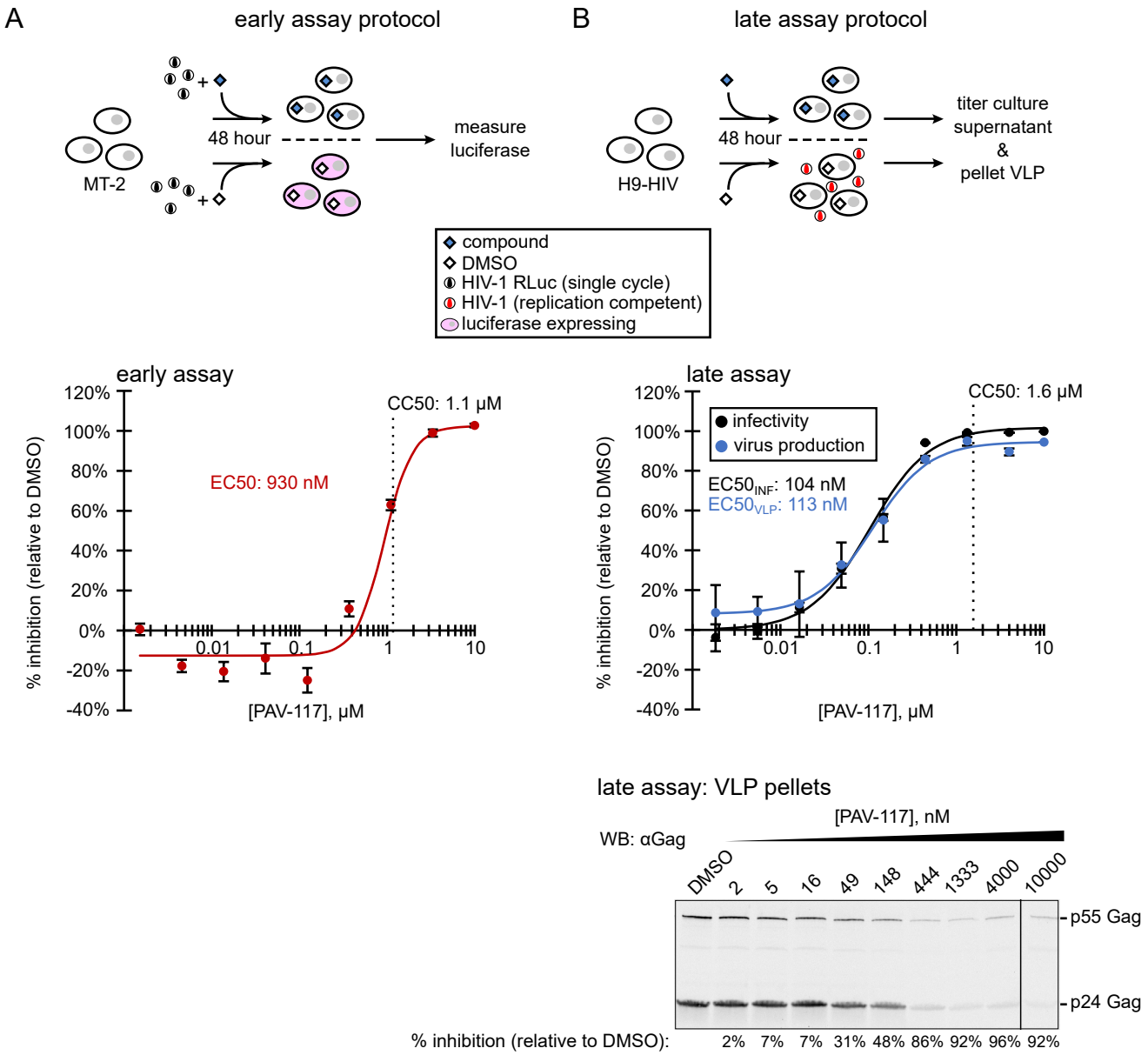

FIG 3 PAV-117 acts late in the HIV-1 life cycle, inhibiting virus production but not specific infectivity.

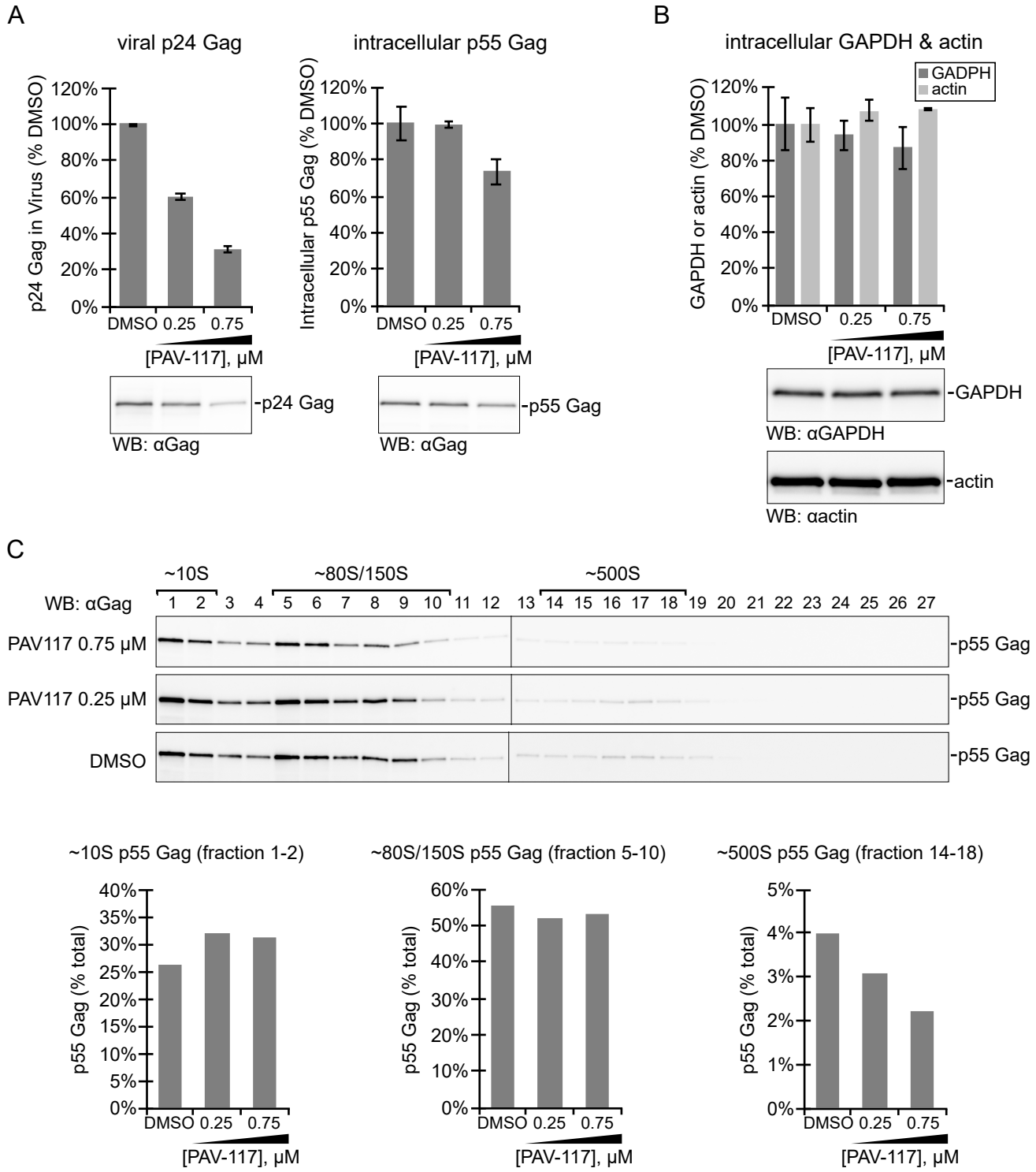

FIG 4 PAV-117 appears to act during the HIV-1 assembly pathway, after formation of the ~80S intermediate.

A

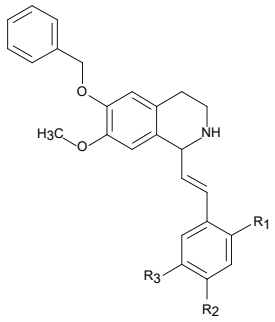

	R_1	R_2	R_3	CC50 (μM)	EC50 (nM)	SI
PAV-117	CH_3	O_{CH_3}	O	1.4 ×/÷ 1.5 (n = 6)	102 ×/÷ 2.1 (n = 5)	14
PAV-218	CH_3	O_{CH_3}	H	9.7 ×/÷ 1.2 (n = 2)	148 ×/÷ 1.1 (n = 3)	66
PAV-220	H	O_{CH_3}	O	3.8 (n = 1)	163 (n = 1)	23
PAV-494	H	H	O	4.1 (n = 1)	244 (n = 1)	17
PAV-493	H	O_{CH_3}	H	21.0 (n = 1)	565 ×/÷ 1.3 (n = 2)	37
PAV-245	CH_3	H	H	3.6 (n = 1)	755 (n = 1)	4.8
PAV-492	H	H	H	> 10 (n = 1)	1540 (n = 1)	> 6
PAV-206	CH_3	O_{CH_3}	O_{CH_3}	2.2 ×/÷ 1.4 (n = 4)	36 ×/÷ 1.1 (n = 3)	61

B

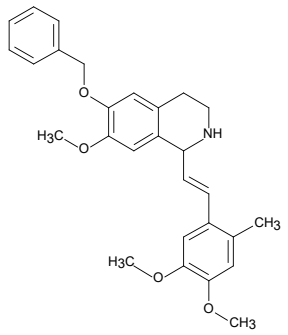

PAV-206

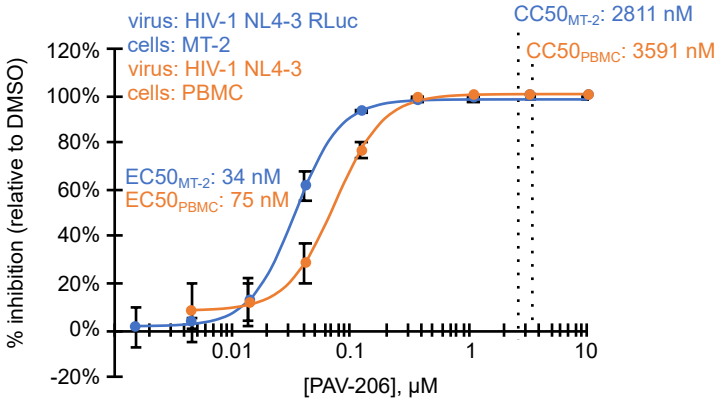

C

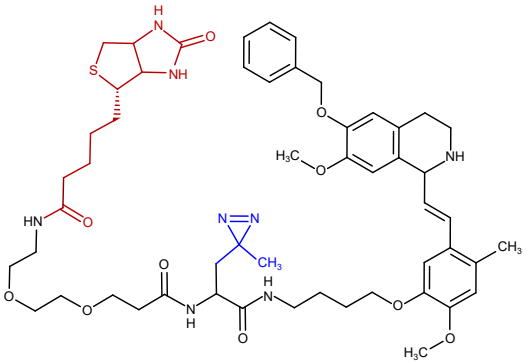

PAV-818

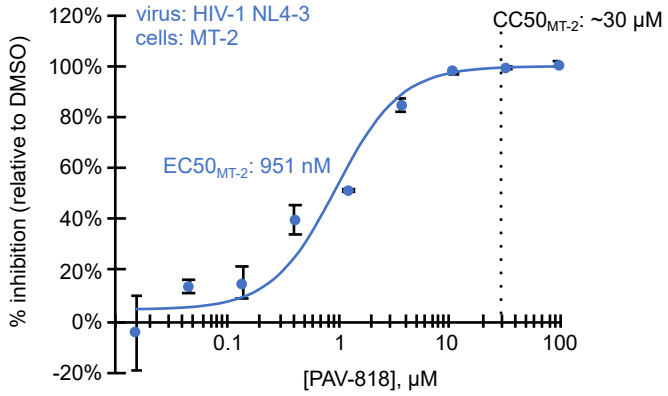

FIG 5 Analysis of structure-activity relationships identified an analog that potently inhibits HIV-1 replication in PBMCs and a site for tags.

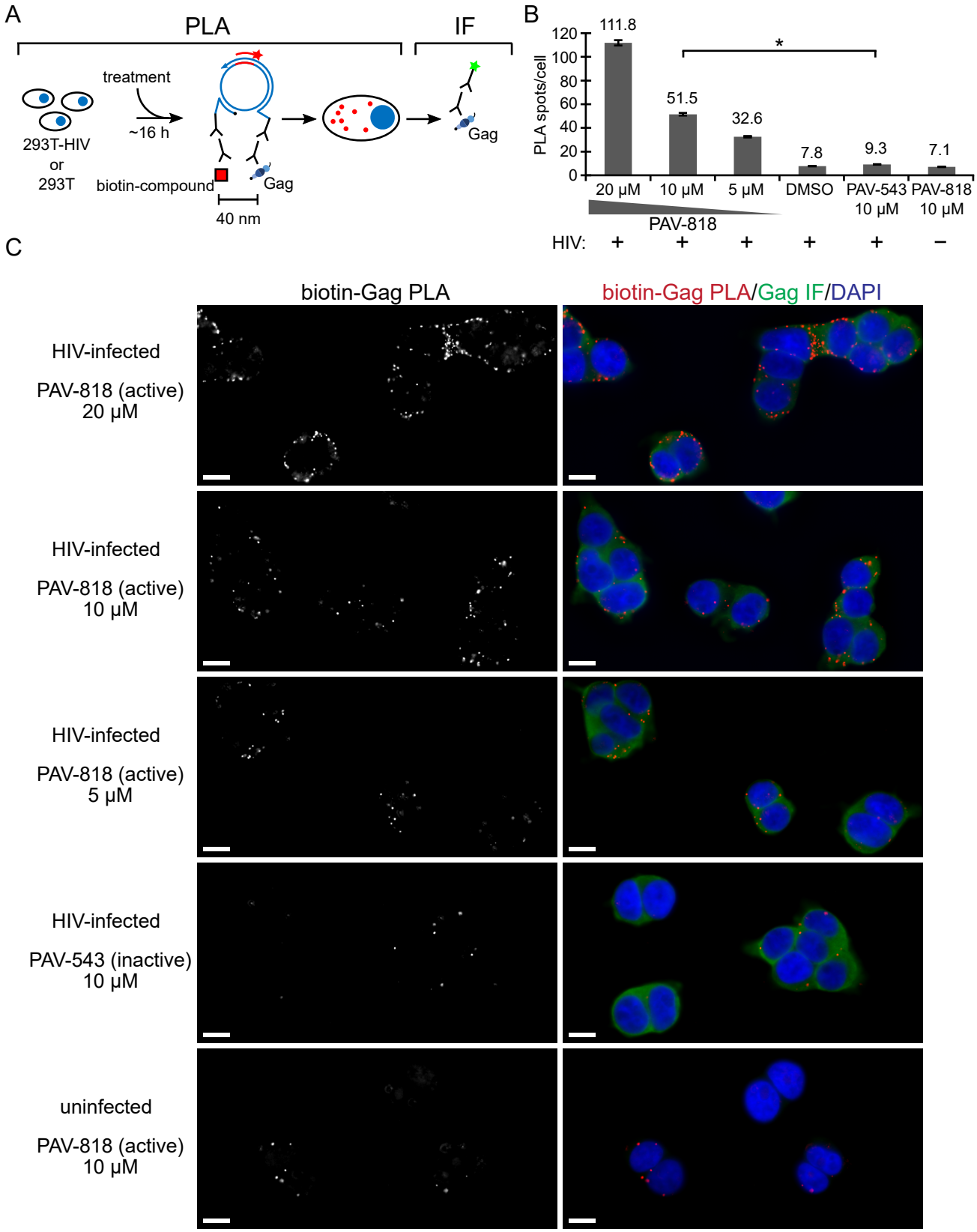

FIG 6 An antiviral analog of PAV-206 colocalizes with HIV-1 Gag *in situ.*

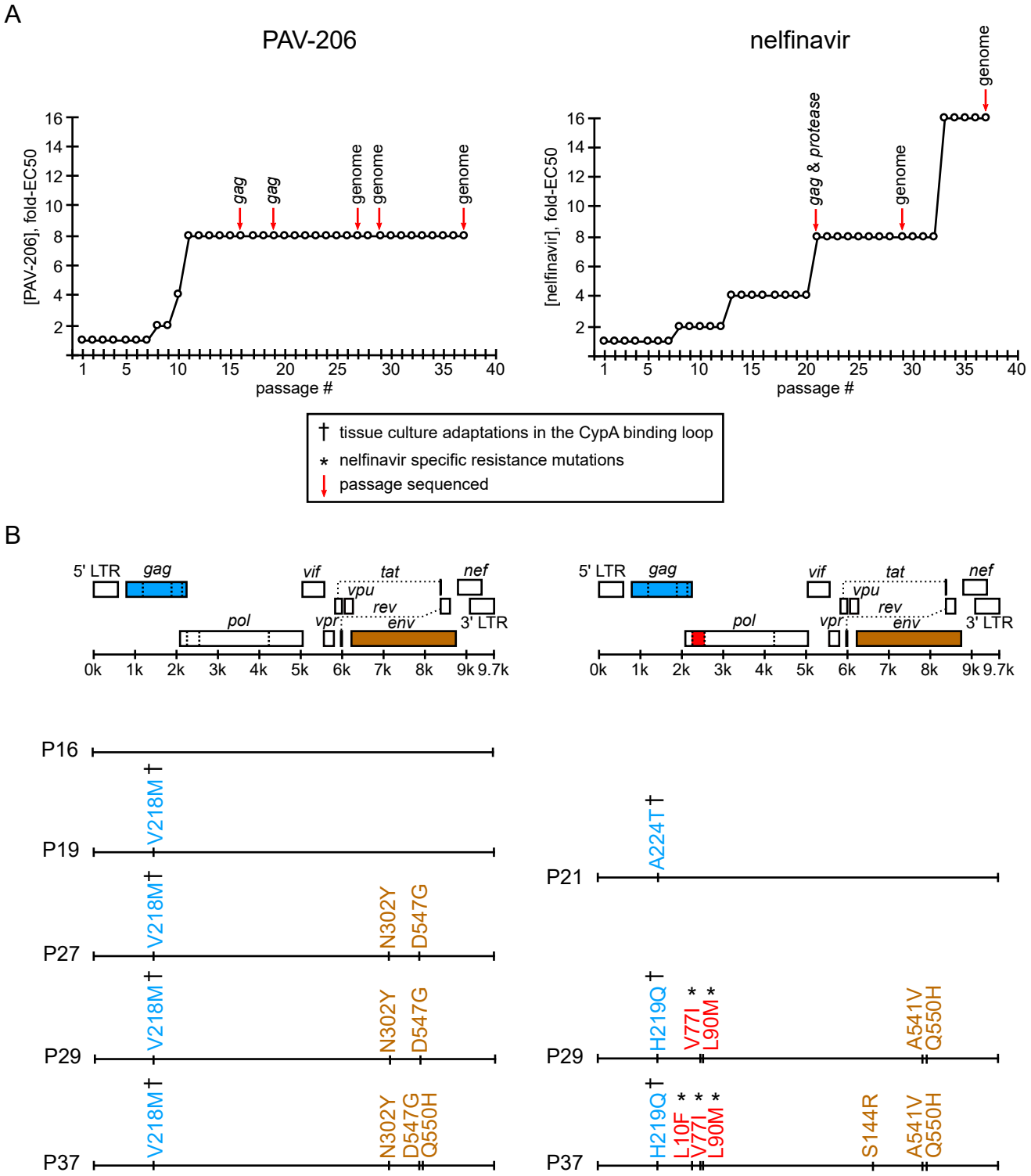

FIG 7 Resistance mutations in *gag* or *pol* were not observed upon selection with PAV-206 in cell culture.

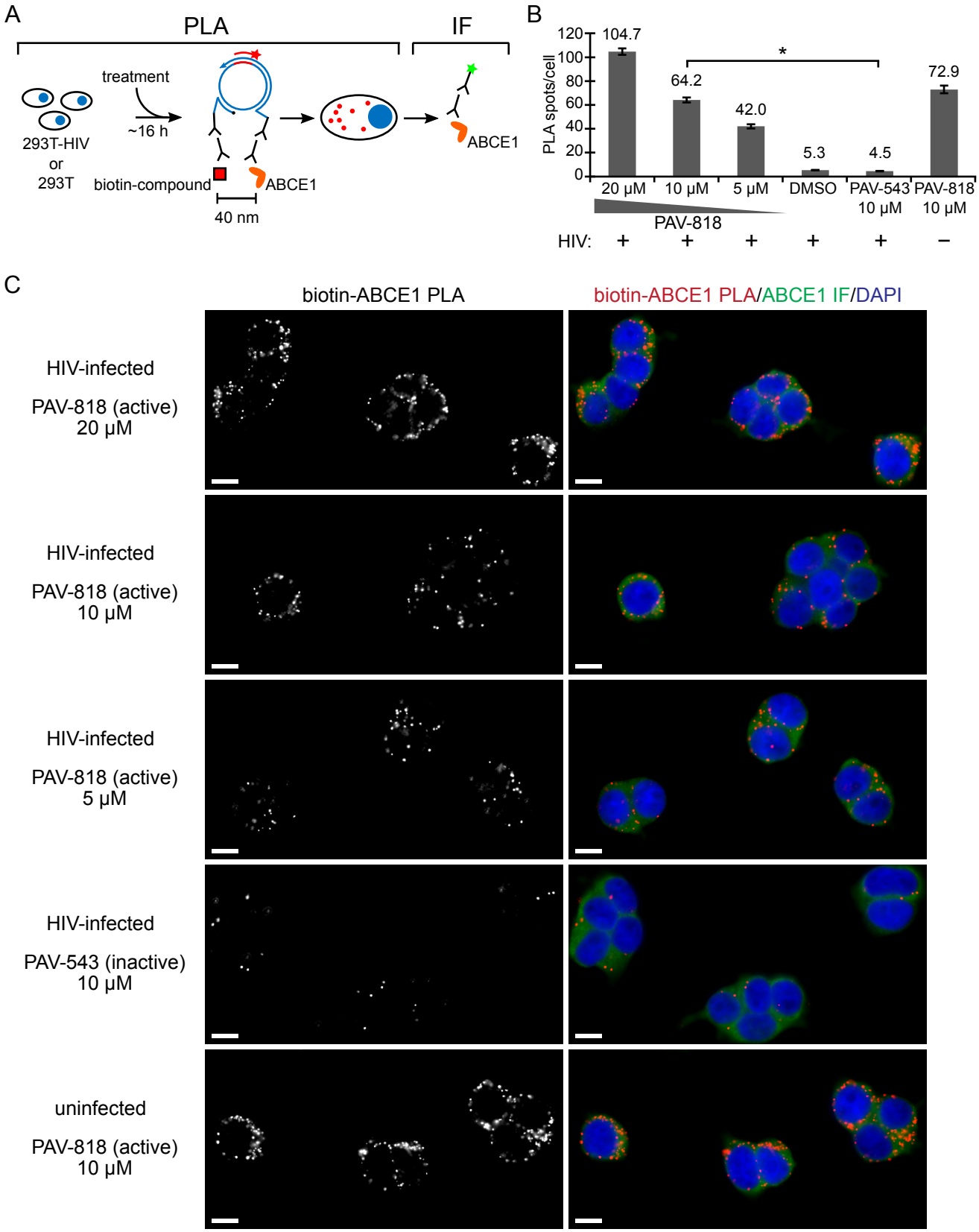

FIG 8 An antiviral PAV-206 analog colocalizes *in situ* with ABCE1, a host component of assembly intermediates.

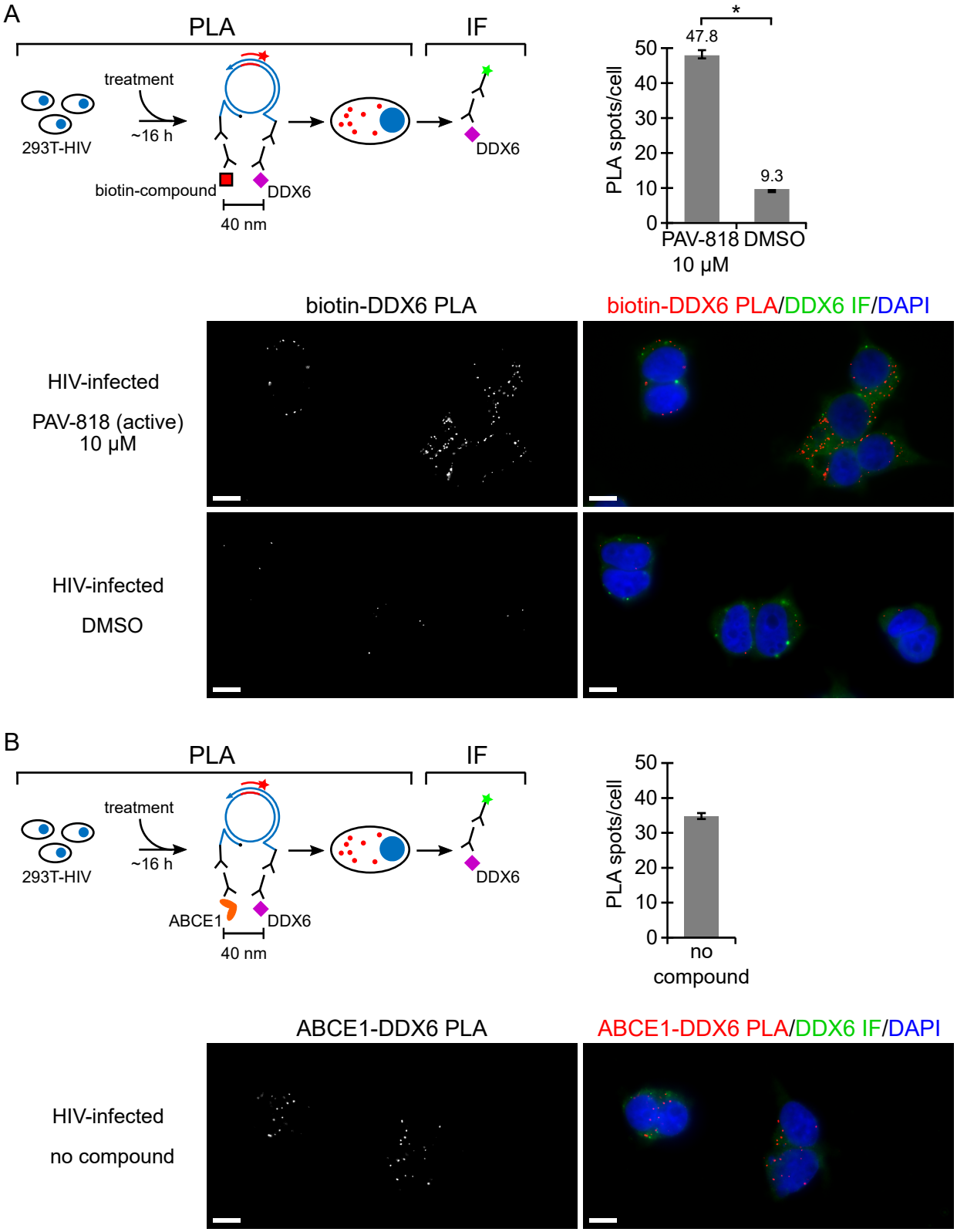

FIG 9 An antiviral PAV-206 analog colocalizes *in situ* with DDX6, an RNA granule protein in assembly intermediates that colocalizes with ABCE1.

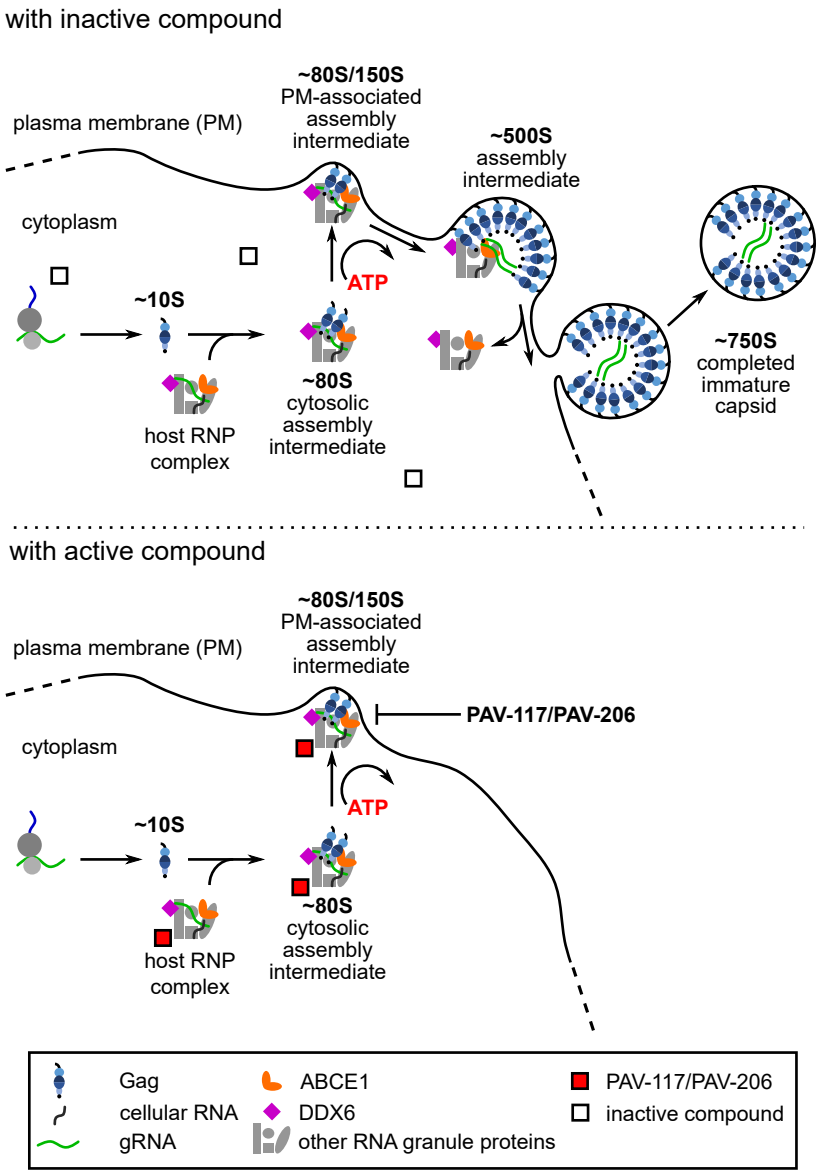

FIG 10 A model for the action of PAV-117 and PAV-206, possible first-in-class selective inhibitors of HIV-1 assembly.

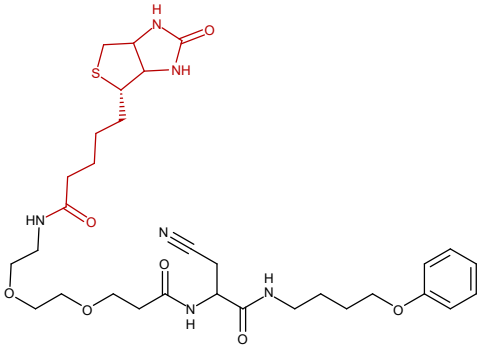

PAV-543

Supplementary FIG 1 Structure of PAV-543, a biotinylated compound that does not have anti-retroviral activity.

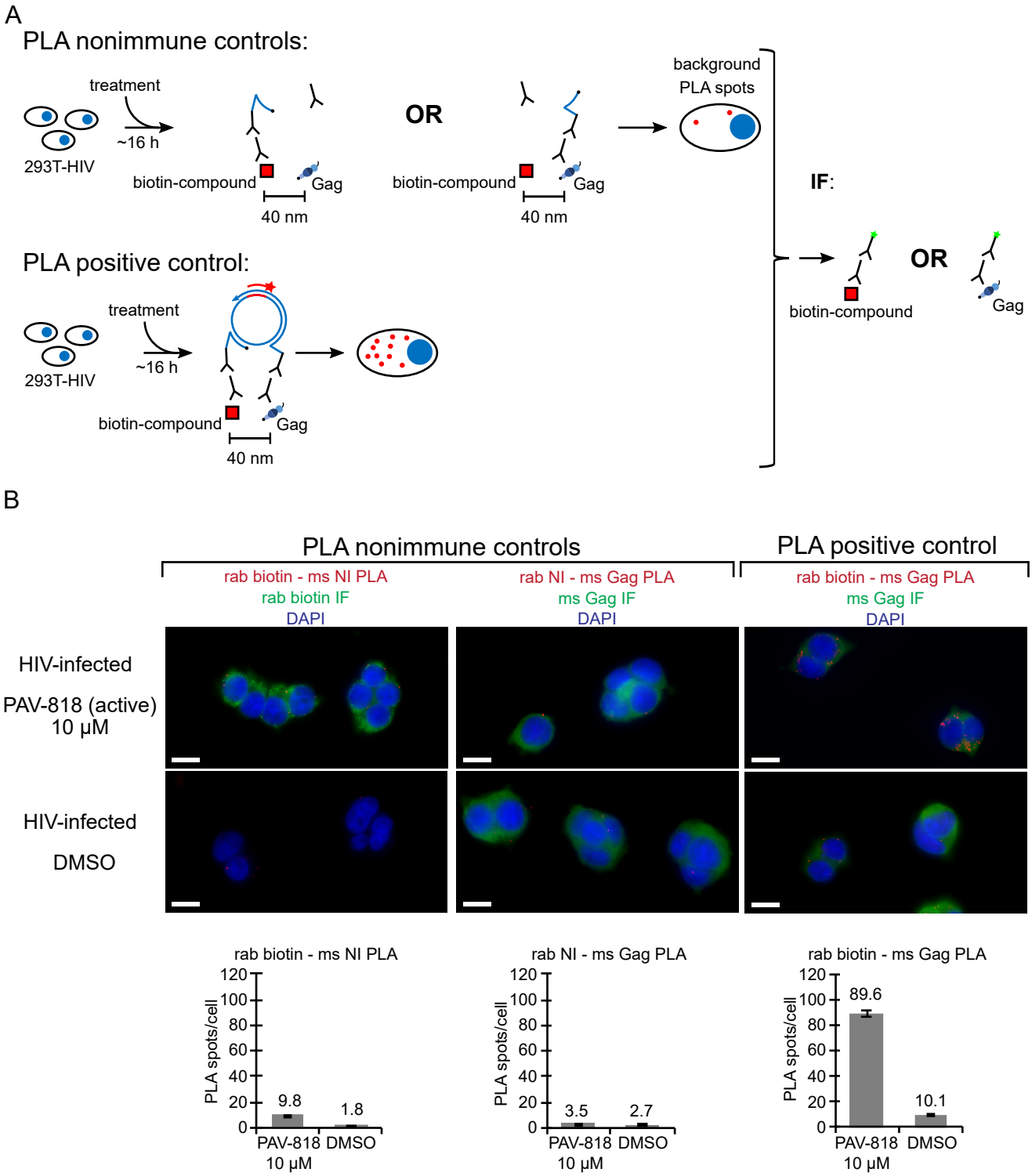

Supplementary FIG 2 Nonimmune controls for the biotin-Gag proximity ligation assay.

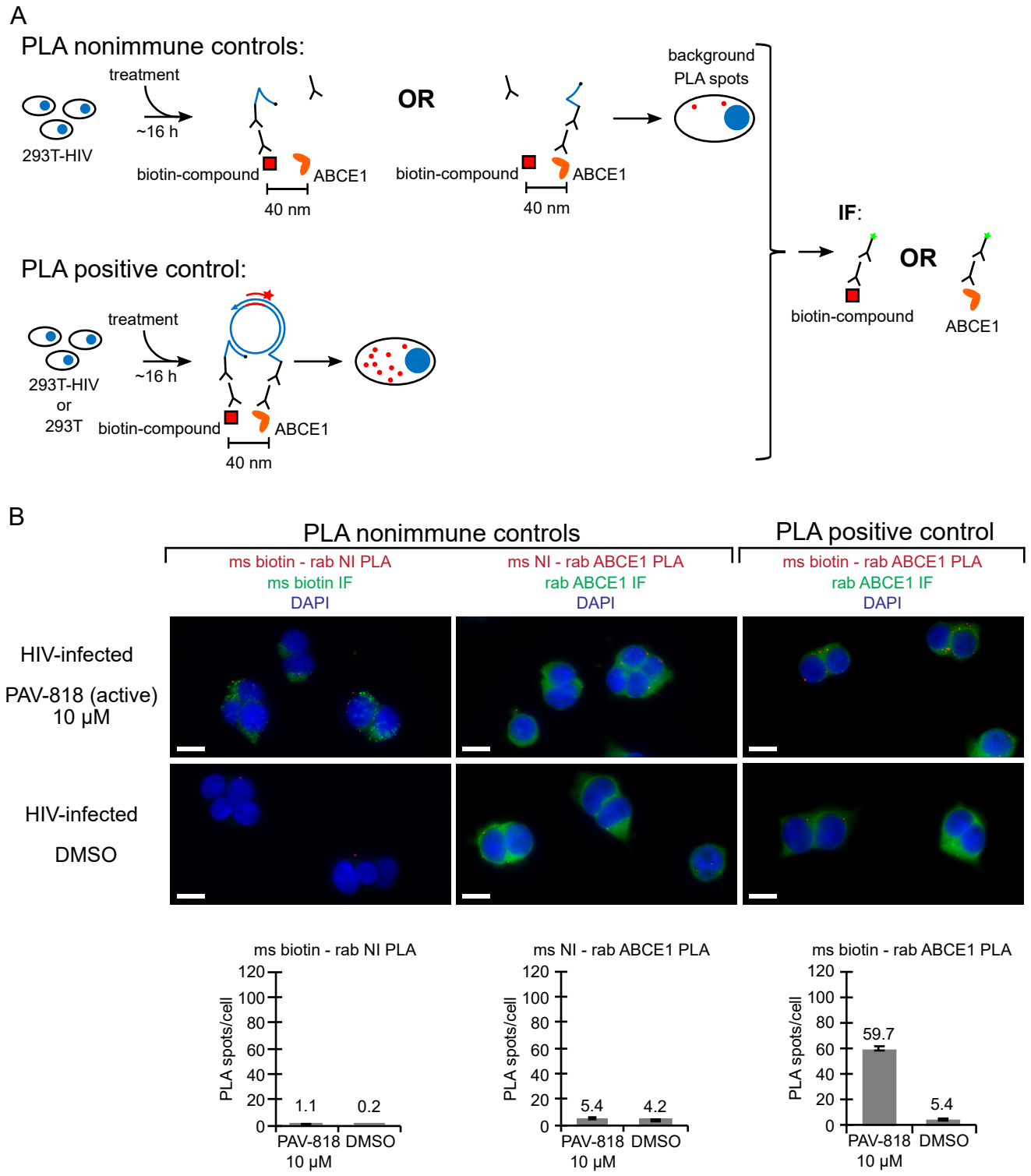

Supplementary FIG 3 Nonimmune controls for the biotin-ABCE1 proximity ligation assay.

SUPPLEMENTARY FIGURE LEGENDS

FIG. S1. Structure of PAV-543, a biotinylated compound that does not have antiretroviral activity. The biotin moiety is shown in red. The EC50 of PAV-543 is > 100 μM in the HIV-1 MT-2 cell spread assay shown in Fig 2C as is the CC50 in MT-2 cells (Reed and Lingappa, unpublished observations), indicating no significant antiretroviral activity.

FIG. S2. Nonimmune controls for the biotin-Gag proximity ligation assay. (A) Schematic of the PLA approach for testing specificity of the antibodies used to determine colocalization of compound with Gag. 293T cells chronically infected with HIV-1 (293T-HIV) were treated with 10 μM PAV-818 (the biotinylated active compound) or DMSO for 16 h. For the positive control, PLA was performed by incubating with primary antibodies (mouse anti-Gag and rabbit anti-biotin) followed by PLA secondary antibodies (anti-mouse IgG coupled to (-) PLA oligo and anti-rabbit IgG coupled to (+) PLA oligo). In the two negative controls, one primary antibody was replaced with a nonimmune control antibody from the same species, as indicated. Addition of other PLA reagents leads to connector oligos linking the (+) and (-) oligos only if the primary antibodies are colocalized; this in turn results in the PLA amplification reaction. Addition of an oligo that recognizes a sequence in the amplified regions and is coupled to a red fluorophore (red star) results in intense red spots at sites where the two primary antibodies are colocalized *in situ*. Thus, red spots indicating colocalization of antigens should be absent when either primary antibody is replaced by a nonimmune antibody. Following PLA, indirect immunofluorescence (IF) is performed by adding a secondary antibody conjugated to a green fluorophore (green star) to detect any unoccupied immune antibody, thus marking Gag-expressing or biotin-containing cells with low-level green fluorescence. (B) A representative field is shown for each of the three antibody pairs and two treatments (the antibodies used are indicated above images, the treatments are indicated to the left). Fields are shown as a merge of three color-channels: the red

26 channel showing biotin-NI PLA, NI-Gag PLA, or biotin-Gag PLA as indicated by red labeling above
27 images; the green channel showing biotin IF or Gag IF as indicated by green labeling above images; and
28 the blue channel showing DAPI-stained nuclei. Scale bars, 10 μm. Graphs below each image column
29 show the average number of PLA spots per cell for each antibody pair and each treatment. Ten to
30 twenty fields were analyzed for each group (containing a total of 107-304 cells per group), with error
31 bars showing SEM.
32
33 **FIG. S3. Nonimmune controls for the biotin-ABCE1 proximity ligation assay.** (A) Schematic of
34 the PLA approach for testing specificity of the antibodies used to colocalization of compound with
35 ABCE1. 293T cells chronically infected with HIV-1 (293T-HIV) were treated with 10 μM PAV-818
36 (the biotinylated active compound) or DMSO for 16 h. For the positive control, PLA was performed by
37 incubating with primary antibodies (rabbit anti-ABCE1 and mouse anti-biotin) followed by PLA
38 secondary antibodies (anti-rabbit IgG coupled to (+) PLA oligo and anti-mouse IgG coupled to (-) PLA
39 oligo). In the two negative controls, one primary antibody was replaced with a nonimmune control
40 antibody from the same species, as indicated. Addition of other PLA reagents leads to connector oligos
41 linking the (+) and (-) oligos only if the primary antibodies are colocalized; this in turn results in the
42 PLA amplification reaction. Addition of an oligo that recognizes a sequence in the amplified regions
43 and is coupled to a red fluorophore (red star) results in intense red spots at sites where the two primary
44 antibodies are colocalized *in situ*. Thus, red spots indicating colocalization of antigens should be absent
45 when either primary antibody is replaced by a nonimmune antibody. Following PLA, indirect
46 immunofluorescence (IF) is performed by adding a secondary antibody conjugated to a green
47 fluorophore (green star) to detect any unoccupied immune antibody, thus marking ABCE1- or biotin-
48 expressing cells with low-level green fluorescence. (B) A representative field is shown for each of the
49 three antibody pairs and two treatments (the antibodies used are indicated above images, the treatments
50 are indicated to the left). Fields are shown as a merge of three color-channels: the red channel showing

biotin-NI PLA, NI-ABCE1 PLA, or biotin-ABCE1 PLA as indicated by red labeling above images; the green channel showing biotin or ABCE1 IF as indicated by green labeling above images; and the blue channel showing DAPI-stained nuclei. Scale bars, 10 μm. Graphs below each image column show the average number of PLA spots per cell for each antibody pair and each treatment. Five fields were analyzed for each group (containing a total of 44 - 77 cells per group), with error bars showing SEM.

SUPPLEMENTARY TABLES

Nelfinavir Selection Results Non-synonymous					
Appearance in sequencing chromatogram*	**Mutation numbered relative to HXB2†**	**Mutation numbered relative to NL4-3†**	**Frequency‡ of amino acids at mutation position**	**Mutation associated with:**	**Notes**
dominant	**H219Q Gag** (H87Q p24 Gag)	H219Q Gag (H87Q p24 Gag)	H 73.31% (6999) Q 22.86% (2182) P 1.73% (165)	culture adaptation to intracellular CypA level (1,2,3); cyclosporin resistance (4)	in the cyclophilin A binding loop
≥ 50%	**A224T Gag** (A92T p24 Gag)	A224T Gag (A92T p24 Gag)	A 67.49% (6443) P 31.35% (2993)	culture adaptation (5)	in the cyclophilin A binding loop
≥ 50%	**L10F Protease** (L66F Pol)	L10F Protease (L66F Pol)	L 85.68% (4451) I 7.10% (369) V 5.47% (284)	nelfinavir resistance (6); other PI resistance (7)	
dominant	**V77I Protease** (V133I Pol)	V77I Protease (V133I Pol)	V 83.10% (4322) I 16.11% (838)	nelfinavir resistance (8,9)	
dominant	**L90M Protease** (L146M Pol)	L90M Protease (L146M Pol)	L 98.77% (5137) M 1.15% (60)	nelfinavir resistance (6); other PI resistance (7)	
≥ 50%	**S144R Env** S114R gp120	S144R Env S114R gp120	S 24.14% (1248) N 21.88% (1131) T 16.12% (833)	fusion inhibitor resistance (10)	in the Env V1 loop
dominant	**A541V Env** A30V gp41	A539V Env A30V gp41	A 94.84% (6728) V 2.93% (208) T 1.97% (140)	culture adaptation (11,12); Rev inhibitor resistance (13)	in the Rev response element
dominant	**Q550H Env** Q39H gp41	Q548H Env Q39H gp41	Q 99.17% (7035)	culture adaptation (11); also arose in PAV-206 selection in current study	in the Rev response element; in the T-20 (Enfuvirtide) drug binding site

* Gel chromatograms were visually inspected to identify a second chromatogram peak that is equal or larger in height than the peak corresponding to the reference sequence (defined here as ≥ 50%) or a single chromatogram peak that differs from the reference sequence (defined here as dominant).
† Indicates viral protein to which numbering refers, either in the HXB2 or NL4-3 HIV strain. Numbering of mutation relative to other relevant proteins or domains is indicated in parentheses. Mutations in bold are shown in Fig. 7.
‡ Determined using AnalyzeAlign (available on Los Alamos HIV databases and compendiums site) using the premade Web Alignment; the top three that are > 1% are listed.

TABLE S1: Mutations that arose upon selection in nelfinavir. Mutations are numbered relative to the HXB2 or NL4-3 genomes, with the frequency of the mutation, the phenotype associated with the mutation, and relevant references indicated.

PAV-206 Selection Results **Non-synonymous**					
Appearance in sequencing chromatogram*	**Mutation numbered relative to HXB2†**	**Mutation numbered relative to NL4-3†**	**Frequency‡ of amino acids at mutation position**	**Mutation associated with:**	**Notes**
dominant	**V218M Gag** (V86M p24 Gag)	V218M Gag (V86M p24 Gag)	V 87.62% (8365) A 4.85% (463) P 3.40% (325)	culture adaptation to intracellular CypA level (14,3)	in the cyclophilin A binding loop
dominant	**N302Y Env** (N272Y gp120)	N300Y Env (N270Y gp120)	N 96.50% (6844) K 1.06% (75)	culture adaptation – CCR5 (15,16,17); fusion inhibitor resistance (18)	in the Env V3 loop; involved in coreceptor binding
dominant	**D547G Env** (D36G gp41)	D545G Env (D36G gp41)	G 99.65% (7069)	replication advantage (19,20); fusion inhibitor resistance (21)	in the Rev response element; in the T-20 (Enfuvirtide) drug binding site; D36 in NL4-3 but G36 in most other strains of HIV-1 (19)
≥ 50%	**Q550H Env** (Q39H gp41)	Q548H Env (Q39H gp41)	Q 99.17% (7035)	culture adaptation (11); also arose in nelfinavir selection in the current study	in the Rev response element; in the T-20 (Enfuvirtide) drug binding site
Synonymous					
≥ 50%	I_{ATT} 205 I_{ATC} Pol (I_{ATT} 50 I_{ATC} Reverse trans.)	I_{ATT} 205 I_{ATC} Pol (I_{ATT} 50 I_{ATC} Reverse trans.)		unknown	
≥ 50%	Q_{CAG} 552 Q_{CAA} Env (Q_{CAG} 41 Q_{CAA} gp41)	Q_{CAG} 550 Q_{CAA} Env (Q_{CAG} 41 Q_{CAA} gp41)		replication advantage (22)	in the Rev response element; in the T-20 (Enfuvirtide) drug binding site
dominant	V_{GTG} 583 V_{GTA} Env (V_{GTG} 72 V_{GTA} gp41)	V_{GTG} 581 V_{GTA} Env (V_{GTG} 72 V_{GTA} gp41)		fusion inhibitor resistance (23)	in the Rev response element

* Gel chromatograms were visually inspected to identify a second chromatogram peak that is equal or larger in height than the peak corresponding to the reference sequence (defined here as ≥ 50%) or a single chromatogram peak that differs from the reference sequence (defined here as dominant).
† Indicates viral protein to which numbering refers, either in the HXB2 or NL4-3 HIV strain. Numbering of mutation relative to other relevant proteins or domains is indicated in parentheses. Mutations in bold are shown in Fig. 7.
‡ Determined using AnalyzeAlign (available on Los Alamos HIV databases and compendiums site) using the premade Web Alignment; the top three that are > 1% are listed.

TABLE S2: Mutations that arose upon selection in PAV-206. Mutations are numbered relative to the HXB2 or NL4-3 genomes, with the frequency of the mutation, the phenotype associated with the mutation, and relevant references indicated.

Supplementary References (for Supplementary Tables)

1. Gatanaga, H., Das, D., Suzuki, Y., Yeh, D., Hussain, K., Ghosh, A., Mitsuya, H. (2005). Altered HIV-1 Gag Protein Interactions with Cyclophilin A (CypA) on the Acquisition of H219Q and H219P Substitutions in the CypA Binding Loop Journal of Biological Chemistry 281(2), 1241-1250.

2. Koh, Y., Amano, M., Towata, T., Danish, M., Leshchenko-Yashchuk, S., Das, D., Nakayama, M., Tojo, Y., Ghosh, A., Mitsuya, H. (2010). In Vitro Selection of Highly Darunavir-Resistant and Replication-Competent HIV-1 Variants by Using a Mixture of Clinical HIV-1 Isolates Resistant to Multiple Conventional Protease Inhibitors Journal of Virology 84(22), 11961-11969.

3. Dicker, I., Zhang, S., Ray, N., Beno, B., Regueiro-Ren, A., Joshi, S., Cockett, M., Krystal, M., Lataillade, M. (2019). Resistance profile of the HIV-1 maturation inhibitor GSK3532795 in vitro and in a clinical study. PloS one 14(10), e0224076.

4. Ptak, R., Gallay, P., Jochmans, D., Halestrap, A., Ruegg, U., Pallansch, L., Bobardt, M., Bethune, M., Neyts, J., Clercq, E., Dumont, J., Scalfaro, P., Besseghir, K., Wenger, R., Rosenwirth, B. (2008). Inhibition of Human Immunodeficiency Virus Type 1 Replication in Human Cells by Debio-025, a Novel Cyclophilin Binding Agent Antimicrobial Agents and Chemotherapy 52(4), 1302-1317.

5. Fadel, H., Saenz, D., Guevara, R., Messling, V., Peretz, M., Poeschla, E. (2011). Productive Replication and Evolution of HIV-1 in Ferret Cells Journal of Virology 86(4), 2312-2322.

6. Patick, A., Mo, H., Markowitz, M., Appelt, K., Wu, B., Musick, L., Kalish, V., Kaldor, S., Reich, S., Ho, D., Webber, S. (1996). Antiviral and resistance studies of AG1343, an orally bioavailable inhibitor of human immunodeficiency virus protease. Antimicrobial Agents and Chemotherapy 40(2), 292-297.

7. Rhee, S., Taylor, J., Fessel, W., Kaufman, D., Towner, W., Troia, P., Ruane, P., Hellinger, J., Shirvani, V., Zolopa, A., Shafer, R. (2010). HIV-1 Protease Mutations and Protease Inhibitor Cross-Resistance Antimicrobial Agents and Chemotherapy 54(10), 4253-4261.

8. Gupta A, Jamal S, Goyal S, Jain R, Wahi D, Grover A. (2015) Structural studies on molecular mechanisms of Nelfinavir resistance caused by non-active site mutation V77I in HIV-1 protease. BMC Bioinformatics. 16 Suppl 19:S10.

9. Chang, M., Torbett, B. (2011). Accessory Mutations Maintain Stability in Drug-Resistant HIV-1 Protease Journal of Molecular Biology 410(4), 756-760.

10. Eggink, D., Bontjer, I., Langedijk, J., Berkhout, B., Sanders, R. (2011). Resistance of Human Immunodeficiency Virus Type 1 to a Third-Generation Fusion Inhibitor Requires Multiple Mutations in gp41 and Is Accompanied by a Dramatic Loss of gp41 Function Journal of Virology 85(20), 10785-10797.

53 11. Nameki D, Kodama E, Ikeuchi M, Mabuchi N, Otaka A, Tamamura H, Ohno M, Fujii N,
54 Matsuoka M. (2005) Mutations conferring resistance to human immunodeficiency virus type 1 fusion
55 inhibitors are restricted by gp41 and Rev-responsive element functions. J Virol. 79(2):764-70.
56 12. Duyne, R., Kuo, L., Pham, P., Fujii, K., Freed, E. (2019). Mutations in the HIV-1 envelope
57 glycoprotein can broadly rescue blocks at multiple steps in the virus replication cycle. Proceedings of
58 the National Academy of Sciences of the United States of America 116(18), 9040-9049.
59 13. Shuck-Lee, D., Chang, H., Sloan, E., Hammarskjold, M., Rekosh, D. (2011). Single-
60 Nucleotide Changes in the HIV Rev-Response Element Mediate Resistance to Compounds That Inhibit
61 Rev Function Journal of Virology 85(8), 3940-3949.
62 14. Gatanaga, H., Suzuki, Y., Tsang, H., Yoshimura, K., Kavlick, M., Nagashima, K., Gorelick,
63 R., Mardy, S., Tang, C., Summers, M., Mitsuya, H. (2002). Amino Acid Substitutions in Gag Protein at
64 Non-cleavage Sites Are Indispensable for the Development of a High Multitude of HIV-1 Resistance
65 against Protease Inhibitors Journal of Biological Chemistry 277(8), 5952-5961.
66 15. Lee B, Sharron M, Montaner LJ, Weissman D, Doms RW. (1999) Quantification of CD4,
67 CCR5, and CXCR4 levels on lymphocyte subsets, dendritic cells, and differentially conditioned
68 monocyte-derived macrophages. Proc Natl Acad Sci U S A 96(9):5215-20.
69 16. Garg H, Lee RT, Maurer-Stroh S, Joshi A. (2016) HIV-1 adaptation to low levels of CCR5
70 results in V3 and V2 loop changes that increase envelope pathogenicity, CCR5 affinity and decrease
71 susceptibility to Maraviroc. Virology 493:86-99.
72 17. Korber B, Gnanakaran S. (2009) The implications of patterns in HIV diversity for
73 neutralizing antibody induction and susceptibility. Curr Opin HIV AIDS 4(5):408-17.
74 18. Hermann FG, Egerer L, Brauer F, Gerum C, Schwalbe H, Dietrich U, von Laer D. (2009)
75 Mutations in gp120 contribute to the resistance of human immunodeficiency virus type 1 to membrane-
76 anchored C-peptide maC46. J Virol. 83(10):4844-53.
77 19. Kinomoto M, Yokoyama M, Sato H, Kojima A, Kurata T, Ikuta K, Sata T, Tokunaga K.
78 (2005) Amino acid 36 in the human immunodeficiency virus type 1 gp41 ectodomain controls fusogenic
79 activity: implications for the molecular mechanism of viral escape from a fusion inhibitor. J Virol.
80 79(10):5996-6004.
81 20. Garg, H., Joshi, A., Blumenthal, R. (2009). Altered Bystander Apoptosis Induction and
82 Pathogenesis of Enfuvirtide-Resistant HIV Type 1 Env Mutants AIDS Research and Human
83 Retroviruses 25(8), 811-817.
84 21. Eggink, D., Langedijk, J., Bonvin, A., Deng, Y., Lu, M., Berkhout, B., Sanders, R. (2009). Detailed

Mechanistic Insights into HIV-1 Sensitivity to Three Generations of Fusion Inhibitors Journal of Biological Chemistry 284(39), 26941-26950.

22. Ueno M, Kodama EN, Shimura K, Sakurai Y, Kajiwara K, Sakagami Y, Oishi S, Fujii N, Matsuoka M. (2009) Synonymous mutations in stem-loop III of Rev responsive elements enhance HIV-1 replication impaired by primary mutations for resistance to enfuvirtide. Antiviral Res. 82(1):67-72.

23. Shimane, K., Kawaji, K., Miyamoto, F., Oishi, S., Watanabe, K., Sakagami, Y., Fujii, N., Shimura, K., Matsuoka, M., Kaku, M., Sarafianos, S., Kodama, E. (2013). HIV-1 resistance mechanism to an electrostatically constrained peptide fusion inhibitor that is active against T-20-resistant strains. Antimicrobial agents and chemotherapy 57(8), 4035-8.

SUPPLEMENTARY METHODS

Synthesis of Tetrahydroisoquinolines

General Procedure for the Synthesis of Substituted Phenethyl amines[a]

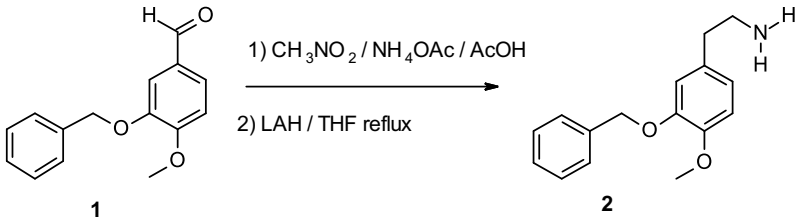

[0001] A solution of the Benzaldehyde **1** (0.1 mol), Nitromethane (50 mL, 0.93 mmol) and Ammonium acetate (0.26 mol) in Acetic acid (200 mL) was refluxed for 1 h. Upon cooling the product crystallized out of solution. The crystals were filtered out and washed with a small amount of ether to give a bright yellow nitrostyrene.

[0002] To a stirred solution of Lithium aluminum hydride (0.21 mol) in Tetrahydrofuran (270 mL) was added dropwise a solution of the above nitrostyrene (0.11 mol) in Tetrahydrofuran (200 mL). Upon completion the reaction mixture was refluxed with stirring for 16 h, cooled to RT and the excess hydride decomposed by the addition of aq. sat. Na_2SO_4. The mixture was filtered and the filtrate rotary evaporated to an amber–brown oil (the title compound) **2** which was used without further purification.

General Procedure for the Synthesis of Substituted Cinammic acids[b]

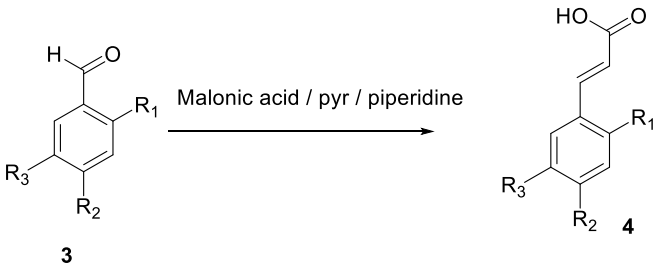

[0003] A mixture of the Benzaldehyde **3** (30 mmol), Malonic acid (60 mmol), Pyridine (20 mL) and Piperidine (5 mmol) was stirred at 80°C for 1 h followed by refluxing at 110-115°C for an additional 3 h. The cooled reaction mixture was poured into water (250 mL) and acidified with conc. HCl. The resulting precipitate was filtered off and washed several times with water. It was redissolved in 2M

NaOH, diluted with water, acidified with conc. HCl. The solid precipitate was filtered washed several times with water, dried under high vacuum over P_2O_5 to afford the titled compound **4**.

General Procedure for the Synthesis of Substituted Cinnamides[c]

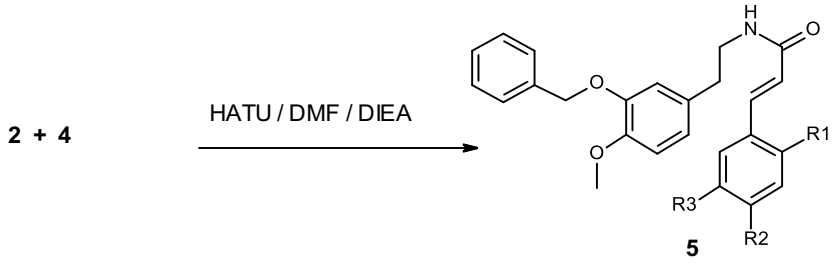

[0004] To a stirred mixture of the substituted Phenethylamine **2** (0.48 mmol), substituted Cinnamic acid **4** (0.72 mmol), DIEA [420 µL (2.4 mmol)] & 10 mL of DMF was added HATU (1 mmol). The reaction was stirred at RT for 1 h and then diluted with 20 mL of EtOAc and washed twice with sat NaCl. The EtOAc layer was dried (Na_2SO_4) and the solvent removed yielding the title compound **5**.

General Procedure for the Cyclization aCOnd Reduction of the Substituted Cinnamides:

Synthesis of Substituted Tetrahydroisoquinolines[d]

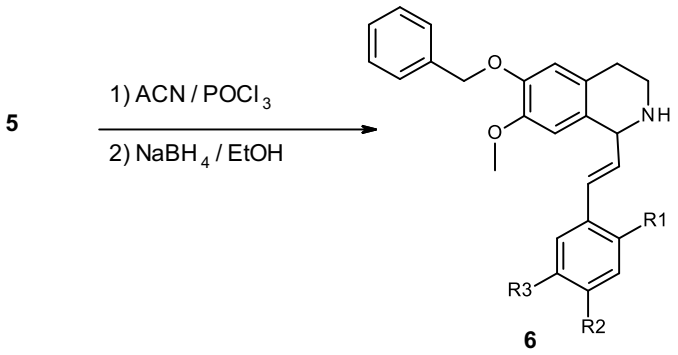

[0005] To the substituted Cinnamide **5** (0.563 mmol) in ACN (13 mL) was added, under reflux, $POCl_3$ (3.9 mmol). The reaction was stirred at reflux for 30 min and then rotary evaporated to dryness. The residue was taken up into 10 mL of chloroform and was then treated with 20 mL of 2N KOH and 50 mL of Et_2O. This mixture was rapidly stirred for 30 min at RT and the upper organic layer removed, washed with water, dried (Na_2SO_4) and the solvent removed. The resulting dark oil (Substituted Dihydroisoquinoline) was then dissolved into 8 mL of dry EtOH and then treated with $NaBH_4$ (0.395

37 mmol). The excess reagent was destroyed by dropwise addition of 2M HCl, basified with 2M KOH and

38 evaporated to dryness to remove EtOH. The residue obtained was partitioned between water and $CHCl_3$,

39 the organic layer was washed with brine, dried (K_2CO_3), filtered, concentrated and purified by flash

40 chromatography using 0.4M NH_3 in MeOH/ $CHCl_3$ gradient (and/or purification via RP C18 Prep HPLC

41 using 0.1% TFA Acetonitrile /water) to afford the titled compound **6**.

42 All compounds were confirmed by Mass Spectrometry:

	R_1	R_2	R_3	M+H (exact mass + H)
PAV117	CH_3	O-CH_3	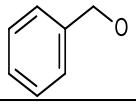	522
PAV218	CH_3	O-CH_3	H	416
PAV220	H	O-CH_3	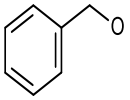	508
PAV494	H	H	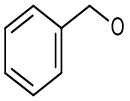	478
PAV493	H	O-CH_3	H	402
PAV245	CH_3	H	H	386
PAV492	H	H	H	372
PAV206	CH_3	O-CH_3	O-CH_3	446

43

44 [a] Cava, M.P.; Buck, K.T. *Tetrahedron* 1969, 25, 2795-2805

45 [b] Nag, Ahindra et al *Journal of Molecular Catalysis B: Enzymatic* **2012**, 82, 92-95; Heo, J.N., et al.,

46 *Bull. Korean Chem. Soc*., 32 (12), 4431, **2011**; Srikrishna, A. et al, *Synthetic Communications*, 37(6),

47 965-976; **2007**.

48 [c] Patent reference: WO2010001169, Astrazeneca.

[d] Herbert, Richard B. et al *Tetrahedron* **1990**, 46, 7119-7138.

Synthesis of N-[2-[2-[3-[[2-[2-[4-[5-[(E)-2-(6-benzyloxy-7-methoxy-1,2,3,4-tetrahydroisoquinolin-1-yl)vinyl]-2-methoxy-4-methyl-phenoxy]butanoylamino]ethylamino]-1-[(3-methyldiazirin-3-yl)methyl]-2-oxo-ethyl]amino]-3-oxo-propoxy]ethoxy]ethyl]-5-[(4S)-2-oxo-1,3,3a,4,6,6a-hexahydrothieno[3,4-d]imidazol-4-yl]pentanamide

Synthesis of 5-(4-bromobutoxy)-4-methoxy-2-methyl-benzaldehyde:

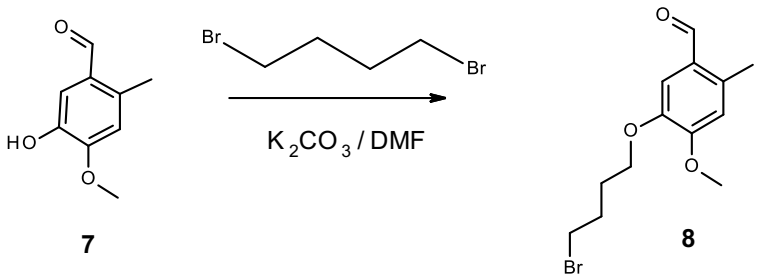

To a solution of Aldehyde **7** [2.7 g (0.016 mol)] in 30 mL of dry DMF was added K_2CO_3 [6.9 g (0.05 mol)]. While stirring at RT under argon atmosphere 1,4-Dibromobutane [10 g (0.048 mol)] was added dropwise. After stirring overnight at RT the reaction mixture was diluted with 100 mL of EtOAc and then washed twice with water. The organic layer was dried (Mg_2SO_4), filtered, and rotary evaporated to dryness to afford 4.1 g the desired Bromide **8**.

Synthesis of 5-(3-azidopropoxy)-4-methoxy-2-methyl-benzaldehyde:

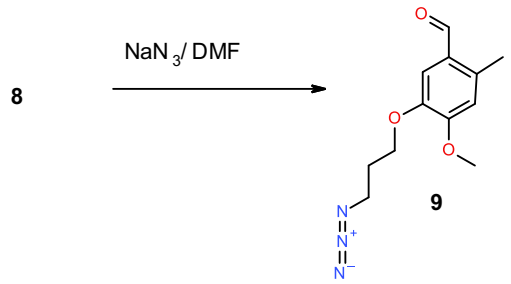

To a solution of Aldehyde **8** [4.1 g (0.014 mol)] in 30 mL of dry DMF was added NaN_3 [1.3 g (0.02 mol)]. After stirring at 70°C under argon atmosphere for 5 h the reaction mixture was cooled and then diluted with 100 mL of EtOAc and followed by washing twice with water. The organic layer was dried (Mg_2SO_4), filtered, and rotary evaporated to dryness to afford 3.3 g (94%) of the desired Azide **9**.

<u>Synthesis of tert-butyl 1-[(E)-2-[5-(4-azidobutoxy)-4-methoxy-2-methyl-phenyl]vinyl]-6-benzyloxy-7-methoxy-3,4-dihydro-1H-isoquinoline-2-carboxylate:</u>

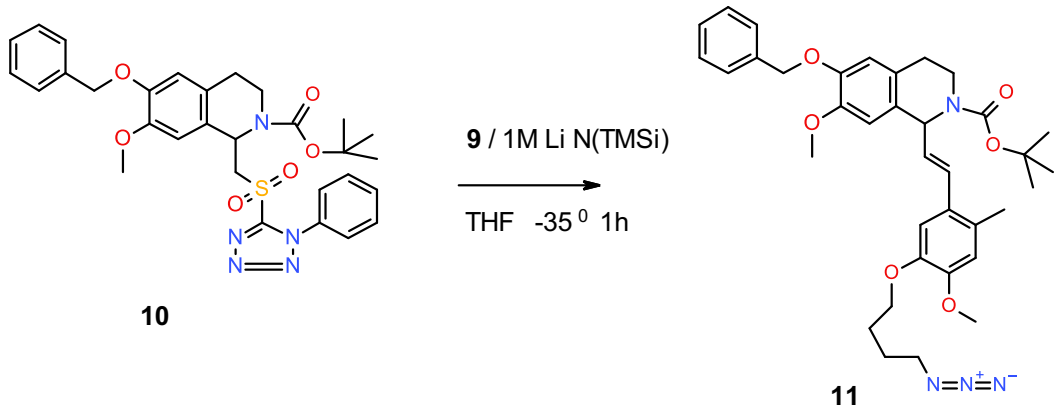

To a solution of Azide **9** [315 mg (1.2 mmol)] in 8 mL of dry THF was added the Tetrahydroisoquinoline **10**[e] [236 mg (0.4 mmol)]. The mixture was then cooled and stirred at −35°C under argon atmosphere. Next 1M LiHMDS in THF [1.2 mL (1.2mmol)] was slowly added dropwise and upon complete addition the reaction mixture was stirred at −35°C for 1 h. The reaction mixture was allowed to come to RT and then quenched with 15 mL of saturated NH_4Cl and then extracted with 20 mL of EtOAc. The organic layer was dried (Mg_2SO_4), filtered, and rotary evaporated to dryness to afford the crude Azide **11**. After flash column chromatography using a gradient of EtOAc / Hexane pure **11** (135 mg) was obtained in 54% yield.

Synthesis of tert-butyl 1-[(E)-2-[5-(4-aminobutoxy)-4-methoxy-2-methyl-phenyl]vinyl]-6-benzyloxy-7-methoxy-3,4-dihydro-1H-isoquinoline-2-carboxylate:

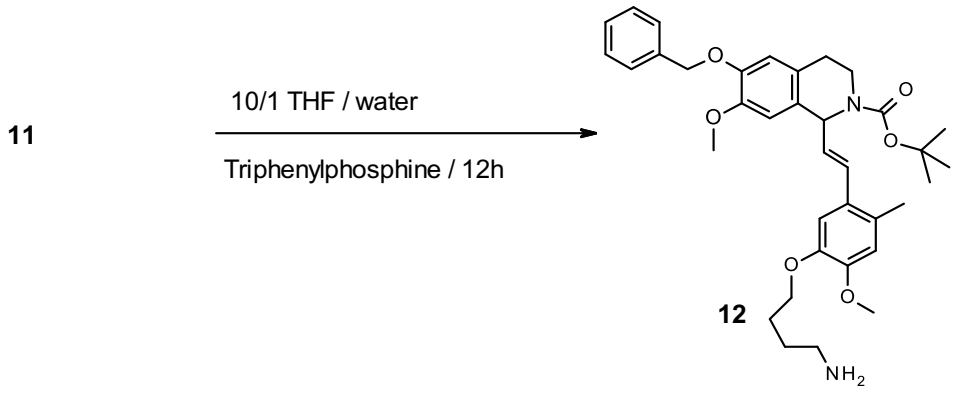

To a solution of Azide **11** [135 mg (0.215 mmol)] in 5 mL of a 10/1 THF / water was added Triphenylphosphine [64 mg (0.25 mmol)]. The reaction mixture was stirred at RT for 12 h. The reaction mixture was then diluted with 10 mL of water and extracted with 20 mL of EtOAc. The organic layer was dried (Mg_2SO_4), filtered, and rotary evaporated to dryness to afford the crude Amine **12**. After flash column chromatography using a gradient of 0.4M NH_3 in MeOH/ $CHCl_3$ pure **12** (90 mg) was obtained in 70% yield.

Synthesis of 3-(3-methyldiazirin-3-yl)-2-[3-[2-[2-[5-[(4S)-2-oxo-1,3,3a,4,6,6a-hexahydrothieno[3,4-d]imidazol-4-yl]pentanoylamino]ethoxy]ethoxy]propanoylamino]propanoic acid:

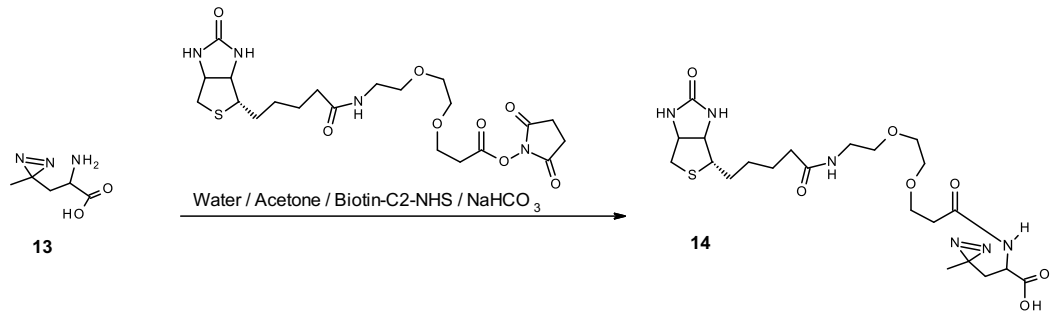

102 To a mixture of Diazirine **13**[f] **[**25 mg (0.17 mmol)], 1 mL Acetone, 1 mL water and $NaHCO_3$ [43
103 mg (0.17 mmol)] was added, with vigorous stirring, Biotin-C2-NHS[f] [85 mg (0.17 mmol)]. The reaction
104 mixture was stirred at RT for 12 h. The reaction mixture was then diluted with 5 mL of water and
105 extracted with 15 mL of EtOAc. The organic layer was dried (Mg_2SO_4), filtered, and rotary evaporated
106 to dryness to afford the crude Acid **14** (40 mg). This was used as was in the next reaction.
107
108 Synthesis of N-[2-[2-[3-[[2-[4-[5-[(E)-2-(6-benzyloxy-7-methoxy-1,2,3,4-tetrahydroisoquinolin-1-
109 yl)vinyl]-2-methoxy-4-methyl-phenoxy]butylamino]-1-[(3-methyldiazirin-3-yl)methyl]-2-oxo-
110 ethyl]amino]-3-oxo-propoxy]ethoxy]ethyl]-5-[(4S)-2-oxo-1,3,3a,4,6,6a-hexahydrothieno[3,4-
111 d]imidazol-4-yl]pentanamide:

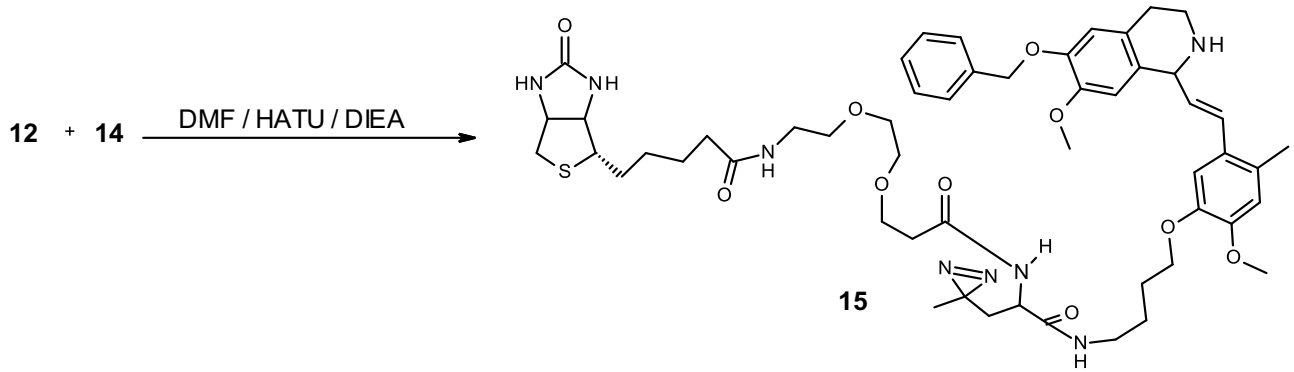

112
113 To a mixture of Acid **14** **[**40 mg (0.076 mmol)] and Amine **12** [(45 mg (0.075 mmol)] was added 1
114 mL of dry DMF and DIEA [35 µl (0.2 mmol)]. Next HATU [38 mg (0.1 mmol)] was added in one
115 portion and the resulting mixture was stirred at RT for 0.5 h. The reaction mixture then diluted with 5
116 mL of EtOAc and followed by washing twice with water. The organic layer was dried (Mg_2SO_4),
117 filtered, and rotary evaporated to dryness. The residue was taken up into 1 mL of Acetonitrile / water (90
118 /10) and then purified on a RP C18 Prep HPLC using 0.1% TFA Acetonitrile /water to afford 17 mg
119 (22% overall) of the desired material **15**. M+H=1013
120 [e] Reddy, R. et al *Journal of Organic Chemistry* 2012, 77, 11101-11108
121 [f] commercially available